3

Wet - Chemically Etched Silicon Nanowire Architectures: Formation and Properties

Vladimir Sivakov[1], Felix Voigt[1,2], Björn Hoffmann[1], Viktor Gerliz[2] and Silke Christiansen[1,3]
[1]*Institute of Photonic Technology, Jena,*
[2]*University of Oldenburg, Institute of Physics, Oldenburg,*
[3]*Max Planck Institut für die Physik des Lichts, Erlangen, Germany*

1. Introduction

In the last years, there is an enormously growing interest in the research and development of silicon nanowires (SiNWs) for various applications in the fields of optoelectronics, photonics and photovoltaics as well as in the sensor field (Cui, 2001; Ross, 2005; Hochbaum, 2005; Schmidt, 2005; Duan, 2001; Kelzenberg, 2008; Stelzner, 2008). The silicon based approaches are certainly favoured because of material abundance and non-toxicity at a high level of materials control and understanding together with a huge industrial infrastructure to account for low production/processing costs and high production yields. The bottom-up fabrication of SiNWs is based on either metal catalyzed growth, known as vapor-liquid-solid (VLS) growth (Givargizov, 1975; Wagner@Ellis, 1964) where metal nanoparticles that form a low temperature eutectic with silicon, such as gold, are liquefied so that they form nanoscale droplets that can be supersaturated from the gas phase with silicon containing species by e.g. chemical vapour deposition (CVD) (Wang, 2006) or physical vapour deposition methods such as laser ablation (Eisenhawer, 2011), molecular beam epitaxy (MBE) (Fuhrmann, 2005; Oh, 2008) or electron beam evaporation (EBE) (Sivakov, 2006, 2007). The growth is carried out with gold (Au) or other metal (Al, Ga, In etc.) (Sunkara, 2001; Civale, 2004) nanoparticles to catalyze the preferred selective axial NW growth at temperatures sufficiently high to form a liquid eutectic with the growth species (Wagner@Ellis, 1964; Lieber, 2003). The first VLS studies were carried out in the 1960s where NW diameters from 100 nm to 100 μm were realized (Givargizov, 1975; Wagner@Ellis, 1964). Today, NWs show diameters in the range between few nanometers up to micrometer scale, with the diameter being determined by the diameter of the metal catalyst nanoparticle (Kamins, 2001; Heath, 1993; Hanrath, 2002; Zhang, 2000; Lauhon, 2002; Xia, 2003; Wagner@Ellis, 1965; Wu, 2000). The schematic representation, shown in Figure 1, illustrates the VLS growth process as it occurs when a particle beam provides the growth species. Vaporized growth species (e.g. silicon atoms or silane (SiH_4) molecules) reach the substrate surface that is covered with metal nanoparticles. The substrate temperature is held above the eutectic temperature of the alloy (here: Au-Si at 373 °C) so that the liquid gold droplet can be supersaturated with silicon atoms. Under the influence of a concentration gradient between the droplet surface and the droplet/nanowire interface, the silicon atoms diffuse to the interface to be incorporated into the silicon nanowire crystal.

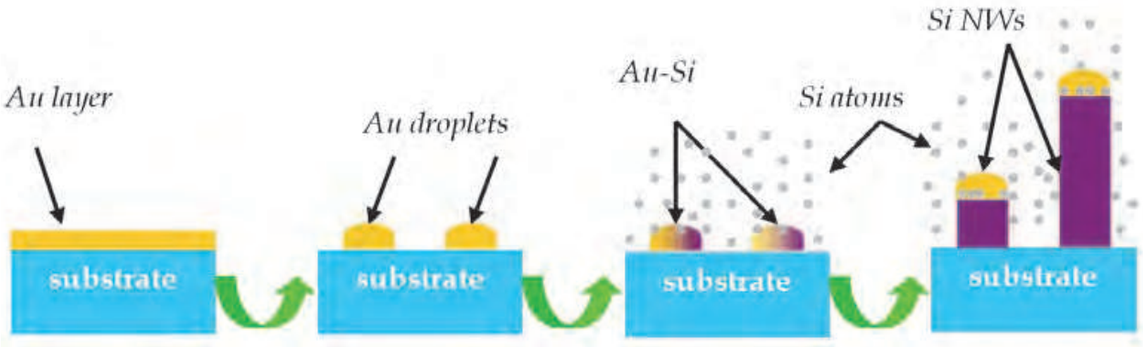

Fig. 1. Schematic drawing of the VLS process as it takes place in a PVD or CVD deposition experiment; first two steps yield the formation of gold droplets by heating of a continuous gold layer on a silicon substrate; third step shows Si atoms to reach the substrate and to be incorporated into the liquid Au-Si droplet above the eutectic temperature (Au-Si: 373°C); and in the last one supersaturation of the Au-Si droplet with Si leads to growth of the SiNW at a higher growth velocity than the continuous silicon layer in between the droplets takes place.

For all device concepts based on SiNWs, the crystal structure, geometry (alignment of SiNW with respect to the substrate), interfacial properties between the SiNW and the substrate as well as the Si core and the shell of the SiNW (either native or thermally grown oxide or a passivating layer like amorphous hydrogenated silicon or silicon nitride), dopant concentrations and impurity levels are of key importance for functioning of the devices. For VLS (bottom-up) grown SiNWs the additional important question arises where and how much metal catalyst (mostly, gold) from the catalyst particle, that initiates the VLS wire growth, resides in the SiNW. However, the enormous impact that even smallest concentrations of Au atoms as a dopant in silicon have a strong influence on optoelectronic properties of the SiNWs makes it essential to understand the extent to which Au atoms diffuse in the SiNW and Si(111) substrate and stay incorporated there and on the SiNW surfaces (Ostwald, 1900). Essentially after it has been shown that the Au from the catalyst is very mobile and diffuses all over the SiNW surfaces and between SiNWs at temperatures as low as 600°C, leading to Ostwald ripening process of Au nanoparticles at the NW sidewalls or even of the NW top Au droplet itself (Allen, 2008; Wagner, 1961; Lifschitz@Slyozov, 1961; Hannon, 2006). VLS approach gives high quality NWs but requires the use of hazardous silane gases at high temperature. Alternatively silicon nanowires can be formed by wet chemical etching method. Metal assisted etching (MAE) has gained an enormous interest in the last time. The technique is based on selective electrochemical etching using catalytic metal and can give ordered and densely packed arrays of high aspect ratio single crystal SiNWs with uniform crystallographic orientations. In a subsequent step, the formation of highly parallel SiNWs with desired lengths, at diameters of the order of few ten nanometers up to a few hundred nanometers could easily be obtained by an aqueous electroless chemical etching of single crystalline silicon wafers (Peng, 2002, 2005, 2006, 2007; Huang, 2008; Qiu, 2005). In this paper we will discuss on the wet chemical etching of SiNWs into a thin silicon layer on glass or single crystal silicon wafer substrates and their optical, optoelectronic and photovoltaic properties.

2. Metal Assisted Wet Chemical Etching (MAWCE)

A catalyst free SiNWs can be realized by electroless wet chemical etching or electrochemical etching into bulk Si wafers or even thin silicon layers (they can be single-, multi-, nano-crystalline or even amorphous) on substrates such as glass (Sivakov, 2009). Engineering flexibility in doping characters of silicon nanowires (SiNWs) is highly desirable to widen the range of their potential applications. Metal assisted wet chemical etching (MAWCE) is a simple and low-cost approach to fabricate SiNWs with designable doping nature. In general, MAWCE can be classified into two types, involving one-step (MAWCE-I) and two-step (MAWCE-II) reactions. In MAWCE, SiNWs are fabricated through non-uniform etching on silicon substrates in aqueous acid solutions, which is catalyzed by electroless deposition of metal nanoparticles on the substrate surfaces (Peng, 2002). This is a simple technique involving only wet chemical processing under the near ambient conditions, leading to a low-cost operation. Note that semiconductor and crystallographic characters of the as generated SiNWs are duplicated from the source substrates by MAWCE. As a result, it may be substantially achievable in MAWCE the flexible engineering of electronic and optical properties in SiNWs. In principle, MAWCE composes of two processes: metal nucleation on silicon substrates by electroless deposition or physical vapor deposition (for example, sputtering), followed by electroless etching of silicon catalyzed by the metal particles. In MAWCE-I only the second step processes consequently occur in an aqueous acid solution containing hydrofluoric acid and hydrogen peroxide. As for MAWCE-II, the metal nucleation is firstly operated in an active aqueous solution for a short period of time, and then the metal deposited silicon surfaces are transferred to another etching solution for SiNW fabrication.

2.1 MAWCE-I

Although MAWCE-I contains only one-step reaction, it is a complex metal catalyzed electrochemical process, involving various critical determinants, such as a concentration of metal ions and etchants, ambient temperature, reaction duration, and nature of source silicon substrates for etching (with relevance to doping character, crystallinity, and crystallographic orientation). The generation of SiNWs using MAWCE-I is involved in simultaneous reduction of metal ions, and oxidation and dissolution of silicon. For instance, aqueous hydrofluoric acid (HF) solution containing silver nitrate ($AgNO_3$) is appropriately selected for etching, and the reaction mechanism has been well studied as following (Peng, 2006). An Ag^+ in the vicinity of the Si substrate captures an electron from Si (eq. 1), causing Ag^0 nucleation on the substrate surface. The electron transfer from Si to Ag^+ is thermodynamically preferential owing to the energy level of the Ag^+/Ag^0 system lying below that of the Si valence band (VB) edges. Accompanying, silicon underneath the Ag^0 nucleus is oxidized into SiO_2 (eq. 2a), which is dissolved by HF (eq. 2b). The dissolution of the electrochemically generated SiO_2 creates a pit underneath the Ag^0 nucleus, and then the nucleus falls into the pit. The excess oxidation causes accumulation of electrons on the surface of Ag^0 nuclei, which attracts Ag^+ in the solution to the vicinity of the nuclei, and the consequent reduction leads to the growth of Ag particles immobilized in the pits on the substrate surfaces. The corresponding reactions can be outlined by (Peng, 2005; Hochbaum, 2009)

$$Ag^+(aq) + e^-_{VB,\,Si} \rightarrow Ag^0\ (solid) \quad (1)$$

$$Si\ (soid) + 2H_2O - 4e^-_{VB,\ Si} \rightarrow SiO_2\ (solid) + 4H^+ \quad (2a)$$

$$SiO_2\ (solid) + 6HF \rightarrow H_2SiF_6 + H_2O \quad (2b)$$

A large amount of Ag^+ in the aqueous solution and Si in the bulk substrate force these reactions occur repeatedly and continuously. As a result, successive deposition of Ag produces a dendrite layer covering the Si substrate, and vertically aligned SiNW arrays are created on the substrate. The vertical alignment is contributed to the longitudinal falling-down of the Ag particles from the surface to the bulk of Si substrates, along with continuous dissolution of Si in the vicinity of Ag particles. The lateral etching along the walls of the generated pores in the bulk Si does not readily take place, because of the longer electron diffusion pathway from the wall to Ag particle comparing to that from the pore bottom underneath the particle. Ag particles play a significant role in catalyzing the cathodic reaction (eq. 1) by effectively lowering the electrochemical reaction barrier. The length of silicon nanowires etched in MAWCE-I is limited to 50 μm at atmospheric conditions (RT, 1 atm), but in the autoclave a length over 50 μm can be reached (Hochbaum, 2008).

2.2 MAWCE-II

Compared to MAWCE-I, the nucleation and electroless etching are operated in two different aqueous solutions in MAWCE-II (Peng, 2005, 2006). The Ag nucleation in MAWCE-II takes place in a $HF/AgNO_3$ aqueous solution, identical to MAWCE-I, followed by etching in a $HF/Fe(NO_3)_3$ aqueous solution. Fe^{3+} is more electronegative than silicon, leading to a cathodic reaction described as

$$Fe^{3+}(aq.) + e^-_{VB,\ Si} \rightarrow Fe^{2+}\ (aq.) \quad (3)$$

This cathodic reaction occurs in the vicinity of the electron-excessive surfaces of Ag particles catalyzed by the particles. The Si underneath the Ag particles is longitudinally dissolved by HF (through eq. 2a and 2b), and continuous occurrence of these reactions produces the vertically aligned SiNW arrays. Note that Ag particles will not dissolved by exchanging electrons with the Fe^{3+}/Fe^{2+} system, contributed from the energy level of the Ag^+/Ag^0 system lying below that of the Fe^{3+}/Fe^{2+} system. The matching in the energy levels effectively facilitates the catalysis of the electroless etching by the Ag particles. Due to the lack of Ag^+ in the electroless etching process, there is no dendrite layer generated on the Si substrates. Electroless etching can be also carried out in a HF/H_2O_2 aqueous solution, with the cathodic reaction given by (Peng, 2007; Zhang, 2008)

$$H_2O_2 + 2H^+ + 2e^-_{VB,\ Si} \rightarrow 2H_2O \quad (4)$$

The substitution of Fe^{3+}/Fe^{2+} with H_2O_2/H_2O to promote the electroless etching is based on the fact that the energy level of the H_2O_2/H_2O system lies far below that of the Si VB edges.

Our chemical etching method to produce SiNWs is based on a two step process, as presented in Figure 2d (Sivakov, 2010). In the first step, Ag nanoparticles were deposited on silicon wafer surfaces by immersing the wafers in aqueous solution of silver nitrate ($AgNO_3$) and hydrofluoric acid (HF) in the volume ratio 1:1 (solution I) for short time. The morphology of the forming Ag nanoparticle deposits is strongly depending on the immersion time. In the second step, silicon wafers covered with Ag nanoparticles of different morphology were immersed in a second etching solution containing HF and 30% H_2O_2 in the volume ratio 10:1 (solution II) for defined time at room temperature.

We show wet chemical etching of silicon wafers involving Ag nanoparticles, HF and H_2O_2 to realize SiNWs of different morphologies depending on processing details, e.g. Ag nanoparticle morphology, silicon wafer orientation (Si(111) and Si(100)). With this control over morphologies at hand we can realize different optical properties of the material to be custom made for optical/photonic devices such as e.g. solar cells. The different SiNW morphologies were investigated using scanning electron microscopy (SEM) as shown in Fig. 2a-c. SiNWs of different regularity and with different orientations could be obtained.

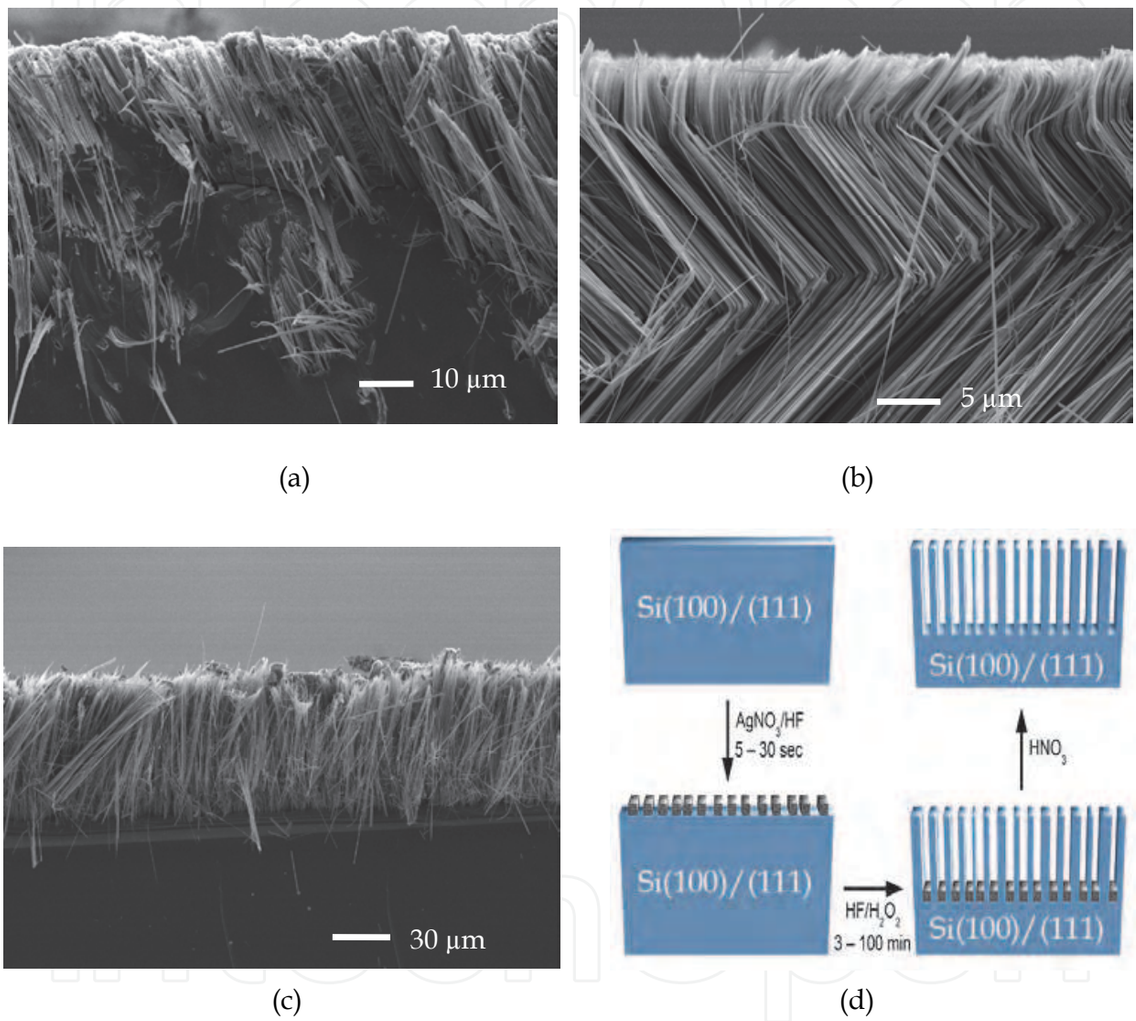

(a) (b)

(c) (d)

Fig. 2. SEM cross sectional micrographs of SiNW arrays formed *via* wet chemical treatment of Si(111) surfaces at: (a) 15s, solution I; 1h, solution II; (b) 60s, solution I; 1h, solution II; (c) 30s, solution I; 1h, solution II. All etching experiments were performed using initial treatment in the 0.02M $AgNO_3$ and 5M HF (solution I) followed by 1h treatment in the second etching agent contained 30% H_2O_2 and 5M HF in the volume ratio of 1:10 (solution II); (d) schematic illustration of the etching process of silicon wafers using a sequence of two solutions; solution I is based on $AgNO_3$/HF and solution II is based on H_2O_2/HF. After solution I treatment, a quasi continuous Ag layer forms on the silicon surface consisting of densely aligning polycrystalline Ag nanoparticles (Sivakov, 2010).

Homogeneous etching profiles and thus regular SiNWs were observed for samples with thicker layers of silver nanoparticles, which form as a result of longer treatment in the $AgNO_3$/HF solution (solution I). Based on these micrographs, it becomes obvious, that the silicon etching homogeneity is strongly depending on the morphology of the Ag nanoparticles/Ag layer. This finding is supported by TEM studies (presented in (Sivakov, 2010)) that show how Ag nanoparticles/Ag layers reside on the silicon wafer surfaces after solution I treatment, prior to solution II etching of SiNWs and also gives information about Ag/Si interface and crystallographic structure.

Our results strongly compared with existing literature data we can state the following: Chen et al. showed wet chemical etching to create SiNWs (Chen, 2008) using Si(100) and Si(110) wafers and some of their results resemble our findings, i.e. they found preferential etching along [100] directions and for changing peculiarities of the etching conditions the Si(111) wafers could also etch along [111] directions, i.e. Si(111) wafers can either be etched perpendicular to the wafer surface along [111] direction or pyramidal along [100] direction. We could show etching of Si(111) wafers for which we can realize straight etching along [111] directions or transition of [111] to [100] directions so that zig-zag architecture in SiNWs forms. To prove the varying etching directions we used electron backscatter diffraction (EBSD) in a SEM. Results of EBSD studies are shown in Fig. 3 and Fig. 4. Due to its excellent spatial resolution of a few 10 nm even over large probed areas, EBSD enables orientation analysis of SiNW with emphasis on grain size (or single crystallinity), grain distribution and SiNW orientations. Fig. 3 proves single crystallinity over the full SiNW length, as given by

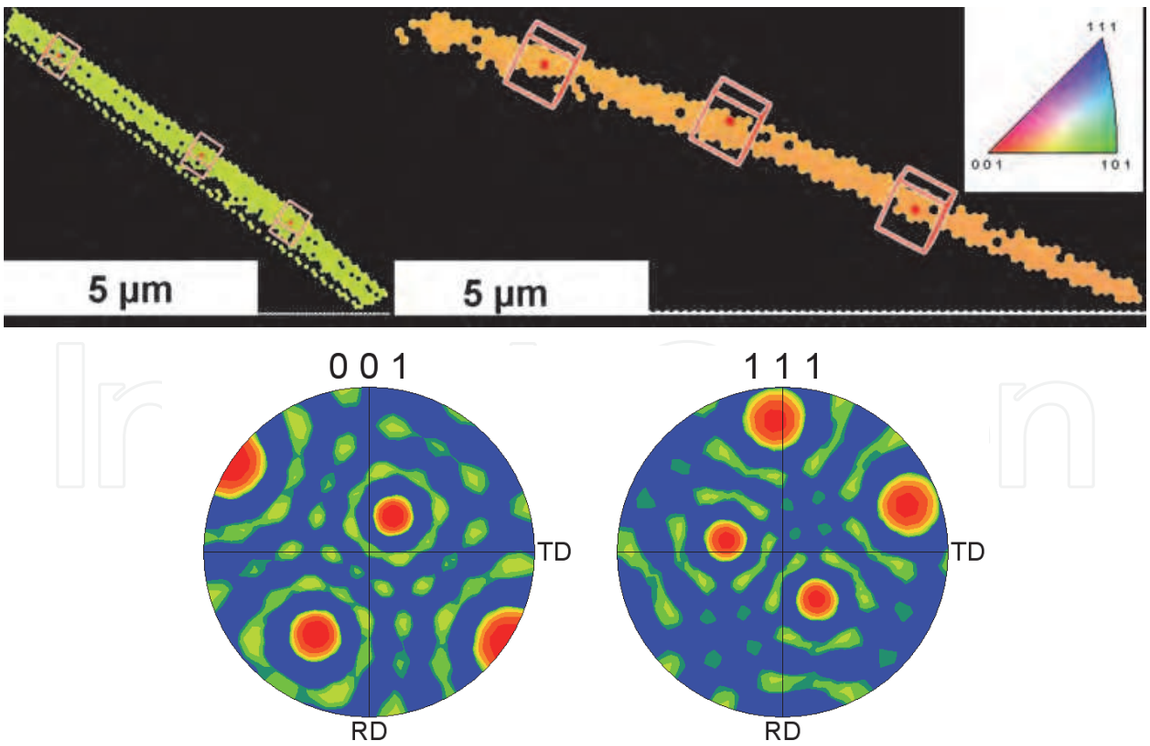

Fig. 3. EBSD analysis (inverse pole figure representation) of two silicon nanorods (SiNRs) fragments etched into a Si(111) wafer. The orientation cubes for both SiNWs show etching direction (parallel to the long axis of the SiNR) to be parallel to [100] direction.

the single colour, coding the SiNW. In contrast to the common use of pole figures for orientation representation in the following the present crystal orientation will be illustrated by orientation cubes showing the orientation of the unit cell with respect to the sample surface. Here every orientation cube belongs to an individual point of the EBSD scan and thus provides only information for the particular point. According to that the determination of small deviations between different points could not be visualized and no statistic about the entire scan could. Nevertheless it provides a direct visualisation of the present crystal orientation and enables an intuitive access to the etching direction. Here it could be shown that etching SiNW from Si(100) wafer results in wires with a long axis almost parallel to the [100] direction. The result of which is displayed by the colour coding of the SiNW surface normal which is a less important number since it shows only how the SiNW is lying on the TEM grid; thus, two SiNWs show different surface normal colour coding in Fig. 3, but identical [100] etching direction as well as the orientation cube that clearly shows the SiNW etching direction to be almost parallel to the [100] direction. In case of vertically etched SiNWs from Si(111) wafers the obtained etching direction is almost parallel to the [111] direction with uniform orientation as shown in Fig. 4.. The over layed orientation cube for this SiNW shows the etching direction to be close to [111]. Small deviations of the expected crystal directions could result from non planar positioning of the SiNW with respect to the TEM grid support.

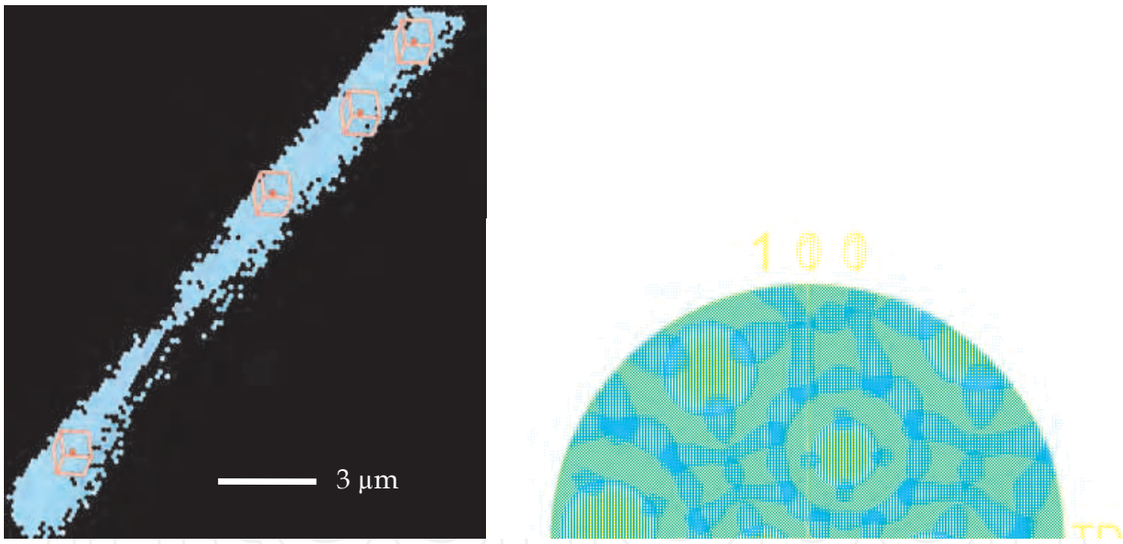

(a) (b)

Fig. 4. (a) EBSD analysis one SiNW fragment of such a wafer; (b) colour coded inverse pole figure representation; the orientation cubes for this SiNW indicate etching direction (parallel to the long axis of the SiNW) to be parallel to the [111] direction.

To support the understanding of the differences in etching morphologies that could be observed we carried out thermodynamic considerations of the different processes. An interesting side effect of the solution I and solution II etching of silicon wafers was, that the processes substantially lead to a heating of the etching solutions from initially room temperature to strongly elevated temperatures of 85°C and above (depending on the used volumes of the solution). Our experiments show that in the first 10 minutes of etching in

solution II (100 ml) the temperature of the solution reached 85°C, after further 15 minutes of reaction time the temperature slowly decreased again reaching room temperature again after 1h. One of the possible explanations of the energy release during the etching procedure in solution II is that a catalytic decomposition of H_2O_2 takes place (Sivakov, 2010). Haber and Weiss (Haber@Weiss, 1935) have investigated the catalytic decomposition of H_2O_2 in homogeneous systems, where the H_2O_2, is primarily attacked monovalently, yielding the active radicals OH^* or HO_2^* (O_2^-) which may further give rise to the chain reactions as shown in Eqs. 5, 6:

$$OH^* + H_2O_2 = H_2O + HO_2^* \quad (5)$$

$$O_2^- + H_20_2 = OH^- + OH^* + O_2\uparrow \quad (6)$$

The catalytic decomposition of H_2O_2 on Ag nanoparticles has also been studied by McIntosh [McIntosh, 1902] and Wiegel. (Wiegel, 1930). These groups have investigated the catalytic decomposition of H_2O_2 in the presence of colloidal Ag. The colloidal Ag partly dissolves in H_2O_2 without appreciable formation of gaseous components according to Eqs. 7, 8:

$$Ag^0 \text{ (solid)} + H_2O_2 = Ag^+ \text{ (aq.)} + OH^- + OH^* \quad (7)$$

$$Ag^0 \text{ (solid)} + OH^* = Ag^+ \text{ (aq.)} + OH^- \quad (8)$$

H_2O_2 is acting as an oxidizing agent in such an environment. Initially, the Ag surface is oxidized, but finally elemental Ag is formed again according to Eq. 9.

$$Ag^+ \text{ (aq.)} + HO_2^- = Ag^0 \text{ (solid)} + HO^* \quad (9)$$

This reaction can take place to a considerable extent, so that elemental Ag and HO_2^* radicals are produced. The latter starts the chain reactions of Eqs. 5 and 6 and give rise to a strong catalytic decomposition of the H_2O_2. As we pointed out in the experimental part, the etching process takes place in an acidic atmosphere by adding 5M HF to the solution. In the case of decomposition in an acidic solution a smaller or greater part of the H_2O_2 is reduced to water without the formation of any gas, according to the equations taken from reference (Weiss, 1935):

$$H_2O_2 + H^+ = H_20 + OH^* + \underline{61 \text{ kcal}} \quad (10)$$

$$OH^* + H^+ = H_2O + \underline{115 \text{ kcal}} \quad (11)$$

As clearly see from Eqs. 10 and 11 during catalytic decomposition of H_2O_2 on Ag nanoparticle surfaces in acidic atmosphere we have a strong exothermal reaction with substantial release of energy that can very well explain the heating of solution II in the first 10-15 minutes of the reaction followed by cooling back to room temperature once the H_2O_2 concentration decreases with reaction time. The substantial temperature rise in the initial 10-15 min of the process may very well influence the preferred etching directions.

In conclusion, we have demonstrated that we can realize homogeneously and reproducibly over large areas SiNW ensembles by wet chemical etching of Si wafers. Different SiNW architectures can be obtained by varying Si wafer orientation and processing peculiarities. Thus, we obtain SiNWs that can either be straight and perpendicular to the wafer surface with a preferred [100] direction of the SiNWs when

using Si(100) starting wafers or zig-zag with orientations varying between [111] and [100] directions when using Si(111) starting wafers. The etching process in acidic atmosphere is a strongly exothermic process thereby heating the etching solution substantially. This process inherent temperature rise is most probably responsible for the change in etching directions with time, thereby allowing the self-organized formation of zig-zag SiNWs. The stabilization and control of straight and zig-zag SiNW formation is very promising to be applied in optical/photonic applications.

3. Absorption, reflectance and transmission

It appears to be obvious that straight and zig-zag SiNWs show different optical properties such as scattering, absorption and transmission of light. As reported before, wet chemically etched SiNWs exhibit a very intense optical absorption (Sivakov, 2009; Tsakalakos, 2007). These wet chemically etched microcrystalline silicon (mc-Si) surfaces show also very low reflectance compared to Si thin layers or wafers (Stelzner, 2008; Andrä, 2007, 2008). This low reflectance is potentially interesting for photovoltaic applications where enough absorption of solar light in an as thin as possible Si layer is desired and a combination of light trapping structures and antireflective coatings have usually to be applied (Peng, Xu, 2005; Kaynes, 2005; Tsakalakos, Balch, 2007). The SiNWs themselves have shown to absorb solar light very satisfactorily and can therefore be used as the solar cell absorber (Tsakalakos, 2007; Tsakalakos, Balch, 2007; Koynov, 2006). The optical reflectance spectra of MAWCE SiNWs etched mc-Si surface on glass and single crystalline wafers as reference are shown in Fig. 5a. The average reflectance of SiNWs realized by wet chemical etching is less than 5% within a range of wavelengths between 300 nm and 1000 nm. The reflectance values (R) are much smaller than those of a polished Si wafer (that shows an R of more than 30%).

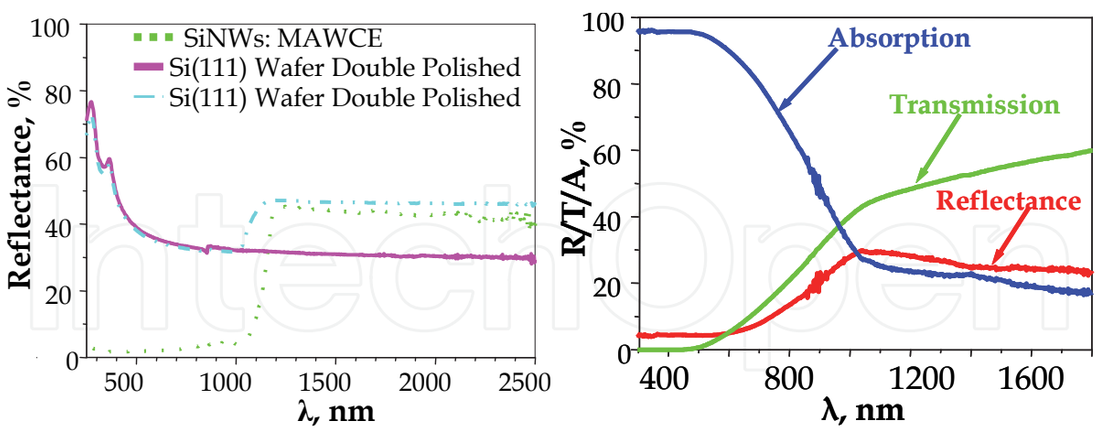

(a) (b)

Fig. 5. (a) Reflectance spectra (Sivakov, 2009) of SiNWs prepared via $AgNO_3$/HF etching of mc-Si layers on glass; as a reference, single or double side polished single crystalline silicon wafers were used; (b) optical transmission (T), reflectance (R) and absorption (A=1-T-R) of SiNWs prepared by etching of mc-Si layers on glass.

The absorption (A) of SiNWs on glass was determined from the optical reflectance (R) and transmission (T) measurements as shown in Fig. 5b. The SiNWs show a very low

reflectance as was also pointed out in Fig. 5a. In the last years, in many reports shown that Si nanostructures can be used as antireflective coatings in solar cells (Tsakalakos, 2007; Andrä, 2007; Tsakalakos, Balch, 2007; Koynov, 2006). Our observation shows the same tendency. On the other hand, it has to be stated that the SiNWs do not transmit light in the range between 300 and 550 nm. This transmission would however be important to use them as antireflection coating on top of a processed solar cell. Moreover, the absorption of mc-Si layers with etched nanowire structures at wavelength > 550 nm was observed to be higher than that of a Si layer of the same thickness. These optical phenomena are selling propositions for the realization of efficient solar cells based on etched SiNWs.

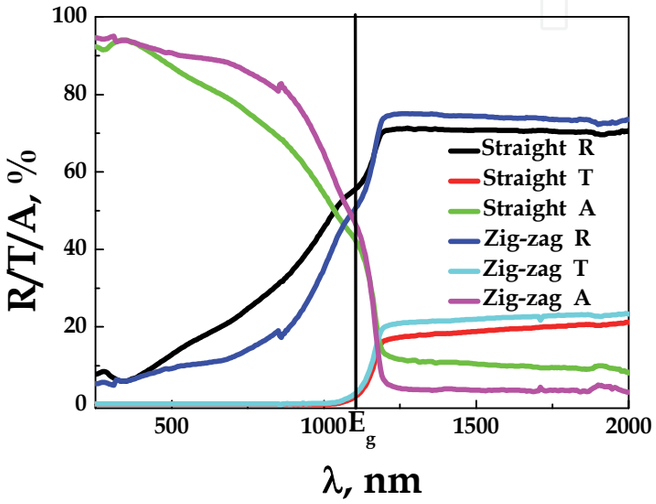

Fig. 6. Reflectance, transmission and absorption spectra of SiNW ensembles with straight and zig-zag SiNWs architecture. The solid line (E_g) indicates the wavelength that corresponds to the Si band gap energy.

Figure 6 shows the comparison results of optical properties of samples with straight and zig-zag SiNWs using an integrating sphere. In the short wavelength range below 1100 nm the reflectance of etched SiNWs is in general low and depends on the morphology of SiNWs, i.e. zig-zag SiNWs and perpendicular SiNWs behave differently as visible from the curves in Fig. 6. The transmission spectra show for short wavelengths (<1100nm) very limited transmission for zig-zag SiNWs and straight, perpendicular to the surface SiNWs. Transmission values increase at higher wavelengths (>1100nm) for both types of SiNWs architectures. The transmission behaviour is important for the use of these SiNWs in antireflection coating applications or absorber layers both to be used e.g. for solar cells. The amount of absorbed light is significantly increased in the zig-zag SiNW material, being important for the aforementioned absorber layer application. As we observed, the absorption of silicon material with zig-zag architecture close to 1100 nm is over 60% and is thus higher than the absorption in the straight SiNWs as shown in Fig. 6.

A significant light absorption was observed in MAWCE-II SiNWs wrapped with aluminium doped zinc oxide (AZO) as shown in Fig. 7. The reflection between two phases with refractive indices n_0 and n_S can be minimized by a thin layer with a refractive index of $\sqrt{n_0 \cdot n_{Si}}$ which gives with $n_0 \approx 1.0$ and $n_{si} = 3.5$ (Jellison@Modine, 1982) an ideal refractive

index of $n_1 = 1.87$, a value close to the value of the deposited AZO (1.85 – 1.90). Furthermore, the AZO surface is not smooth but rough, as shown in Figure 22b, from crystallites that assume the shape of half-spheres. This roughness introduces a kind of moth-eye-effect (Wilson@Huntley, 1982) and thus leads to even increased absorption. Due to the metallic back contact the solar cells do not show any transmission in the investigated wavelength area from 300 to 1500 nm, therefore the absorption A is calculated by A=1-R. The average reflectance of wet-chemically etched SiNWs wrapped with AZO is less than 10% within a range of wavelengths between 300 nm and 1050 nm. Such silicon naostructures show over 90% absorption in the range between 300nm and 1050 nm. We have also demonstrated that lowly and heavily doped SiNWs from wet chemical etching of single crystalline silicon wafers can strongly emit visible photoluminescence at room temperature (Sivakov, Voigt, 2010). These optical phenomena are selling propositions for the realization of efficient solar cells based on etched SiNWs.

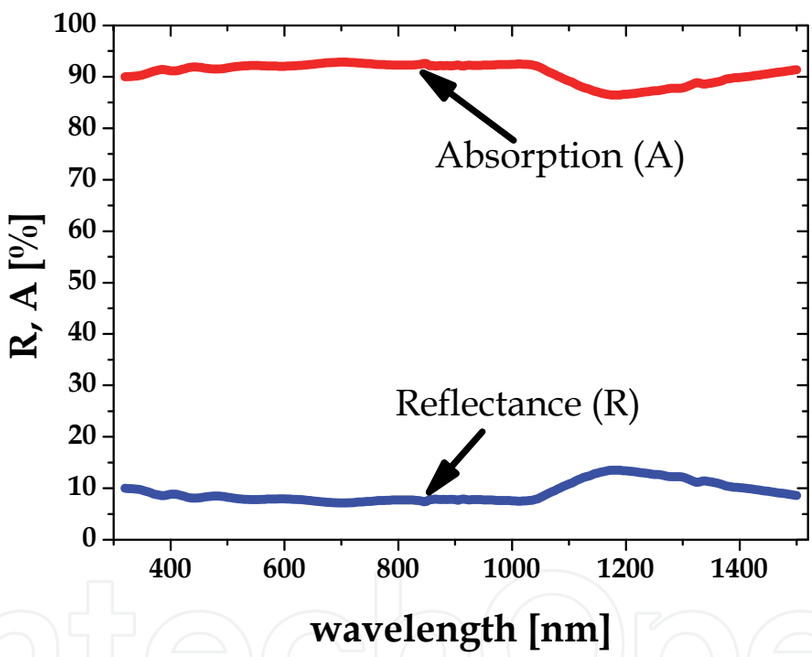

Fig. 7. Optical reflectance (R) and absorption (A=1-R) of semiconductor-insulator-semiconductor (SIS) solar cells based on wet chemically etched SiNWs.

4. Room temperature photoluminescence

4.1 Photoluminescence background

Enormous interest of the scientific community in the photoluminescence (PL) of Si based nanostructured silicon started, after the formation of porous silicon was realized and strong visible PL was observed (Canham, 1990). The material was obtained by anodic oxidation of crystalline Si wafers in diluted hydrofluoric acid (HF). It involves an electrochemical process, where the Si wafer serves as anode and another material is immersed as cathode within the solution. First reports of anodically etched porous silicon (AE-PSi) were

published by Uhlir (Uhlir, 1956). This publication concentrated on electrolytic shaping of Ge and Si and especially on the formation of etch pits, but did so far not mention the strong visible PL of AE-PSi, which at a later date, highly excited the scientific community. Only after the next step in porous silicon (PSi) history - the report of the discovery of strong visible PL of AE-PSi (Canham, 1990) – a real drive in the exploration of optoelectronic properties of AE-PSi started. Canham et al. attributed the PL emission at super band gap energies to the formation of quantum wires within the etched Si layer. For crystalline silicon (c-Si) the room temperature (RT) band gap amounts to $E_{g,c\text{-}Si}$ = 1.12 eV. The PL light emission in the visible range of the spectrum highly excited scientists in the field of semiconductor physics, because with this discovery one goal in the direction of building a visible range silicon LED was reached, a device which was still missing. Overall practical aim mentioned in Canham's above cited publication was the reduction of the extremely large intrinsic radiative lifetime of c-Si in order to make it feasible for light emitting devices and the followed approach for realization was the introduction of quantum confined states in silicon by anodic etching. But, so far no microscopic evidence of the hypothesis of quantum confined states as source of the found PL in the photon energy range 1.4 eV to 1.6 eV had been given by Canham, the existence of quantum confined states in AE-PSi was still a working thesis.

Contemporaneously, Lehmann and Gösele (Lehmann, 1990) published a similar hypothesis about the presence of quantum wires, resulting in quantum confinement effects in AE-PSi. But, in contrary, they concluded this result from optical transmission measurements on the etched layers, and not from PL measurements. Further strong hints to support their hypothesis were drawn from comparison of AE-PSi produced from degenerate initial Si wafer material with non-degenerate p-type silicon. For degenerate wafers, larger structures with dimensions in the range of the depletion width in the Si material – when forming a junction with the surrounding HF etchant – were found by transmission electron microscopy (TEM) and smaller structures were detected for AE-PSi obtained from p-type, non-degenerate wafers. The diameter ranges observed were further affirmed by gas adsorption measurements, by means of which the porosity of the material was estimated. The formation of wires with different diameters was explained by a model, assuming that for degenerate wafers complete depletion of the pore walls stops the etching process, whereas for p-type, non-degenerate wafers a self-limiting process occurs, which is due to quantum wire formations including band gap energy shifts. And band gap energy shifts related to quantum confinement happen at much smaller wire diameters than the depletion width inside degenerate wafers. These observations of wire diameters in complementation with investigations of absorption on AE-PSi formed from different types of initial wafers were again in agreement with the quantum confinement hypothesis in the wires. It was found that AE-PSi formed from degenerate wafers does not show quantum confinement related features in absorption measurements, whereas material formed from p-type, non-degenerate wafers did.

In the following years this initial hypothesis of quantum wire PL in AE-PSi was critically challenged and other hypotheses for the origin of the high energy PL in the material arose. These hypotheses can roughly be summarized as follows:

A Quantum confinement effects within quantum wires
B Quantum confinement effects within quantum dots (nanocrystals)

C Surface and interface effects, e.g. in the Si/SiO_x boundary interfaces or more generally in the surface region

Models A and B both belong to the quantum confinement hypothesis, applied to 1D and 0D structures, respectively. Model C implies a large number of possibilities, because surfaces and interfaces of nanostructured silicon very sensitively depend on the method of preparation. There are a lot of possibilities of SiO_x compounds and structures, which can lead to PL in the visible range of the spectrum. Overall, one can conclude from publications and review articles on this field, that all three hypotheses (A, B, C) are appropriate, but which one applies in each cased depends on the exact microscopic and nanoscopic structure of the AE-PSi sample under investigation. For the hypothesis A and B more detailed specification of the models is not necessary here, they are sufficiently well defined by the sentences above and sketched in Figures 8a, b. There exist many publications on methods to prepare precisely defined single silicon nanowires (SiNWs) (e.g. Peng, 2002; Hochbaum, 2009; Qu, 2009; Sivakov, 2009; Stelzner, 2008) or silicon nanocrystals (Si-NCs) (e.g. Ehbrecht, 1995) and also a lot of publications about PL originating from single SiNWs (e.g. Walavalkar, 2010) or Si-NCs (Huisken, 2002; Ledoux, 2002). Basis of most of the PL studies on these low dimensional single structures is mostly a quantum confinement effect, which induces an energy shift of the emission peak with respect of the RT band gap of silicon.

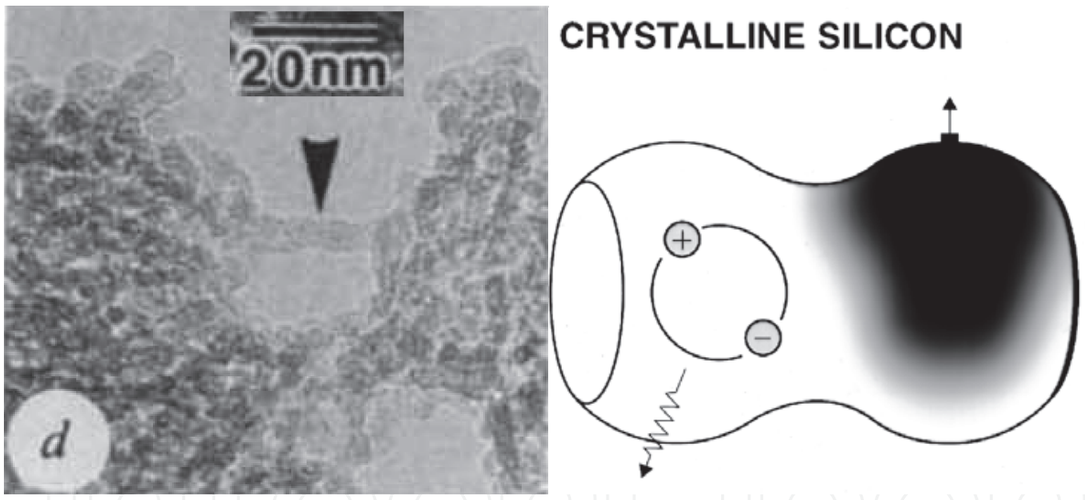

(a) (b)

Fig. 8. PL generation in nanostructured Si due to quantum confinement effects. (a) Quantum wire as seen by TEM in an AE-PSi sample, referring to hypothesis A; Reprinted by permission from Macmillan Publishers Ltd: nature (Cullis, 1991), copyright 1991. (b) Nanocrystals or homomorphous, near 0-dimensional structures, referring to hypothesis B; reprinted with permission from (Cullis, 1997). Copyright 1997, American Institute of Physics.

There have been proposed numerous models for the origin of visible PL, belonging to hypothesis C. Many of them were summarized in the review article (Cullis, 1997). We will further roughly follow this review article in order to discuss the main issues thereof. Fig. 9 shows four possible sources of PL origin as discussed in (Cullis, 1997), which we will discuss in the following paragraphs.

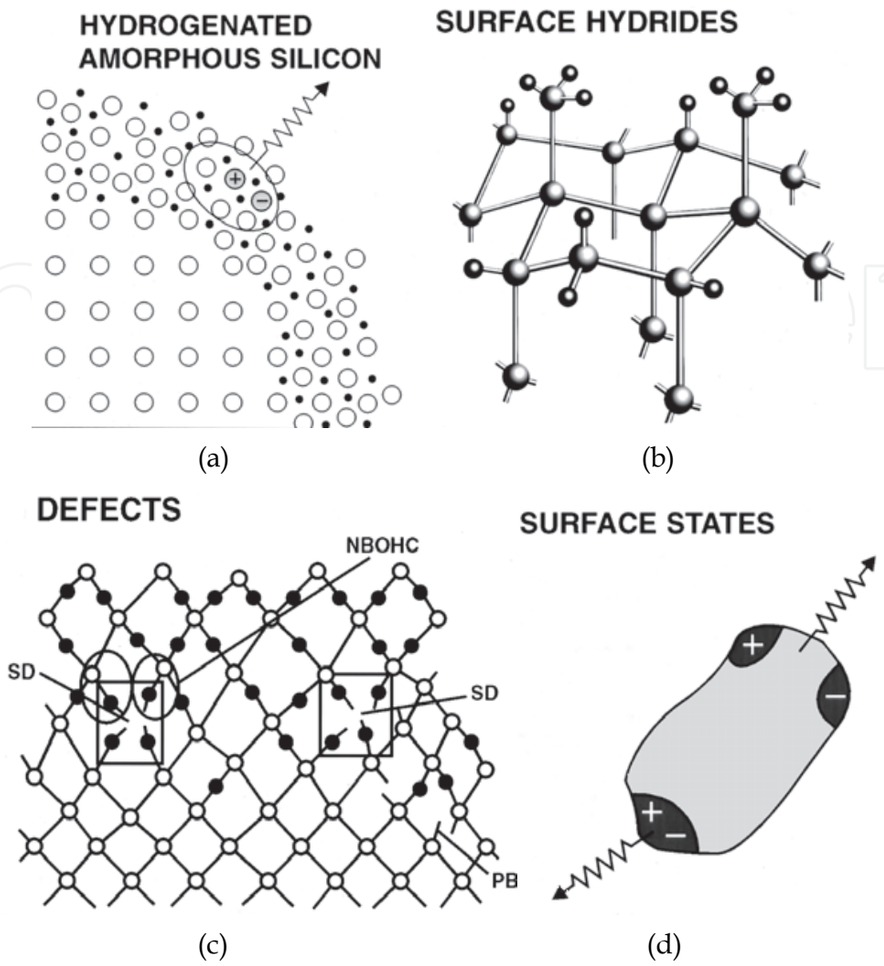

Fig. 9. Four models of PL origin belonging to hypothesis C. Reprinted with permission from (Cullis, 1997). Copyright 1997, American Institute of Physics. Part (d) was initially adopted from (Koch, 1993) and is reproduced with permission by Cambridge University Press.4.1.1 Hydrogenated amorphous silicon

Hydrogenated amorphous silicon (a-Si:H) can be formed on the surfaces of the porous material (Street, 1991). In the transition region between the crystalline cores of the porous material and the surface, nonstoichiometric silicon oxide (SiO_x) is formed. This region usually is of amorphous structure, and in the presence of hydrogen atoms during the preparation process, also incorporates H-atoms. The presence of H-atoms is true in the case of AE-PSi, as the Si surfaces immediately after removal from the dilute hydrofluoric acid are known to be hydrogen terminated (Kolasinski, 2009). It is known that a-Si:H possesses a PL band with peaks in the photon energy at 1.3 to 1.4 eV (Carius, 2000). In the following, if we speak about energy ranges in PL emission, always the ranges of the peak positions are denoted. Furthermore, PL emission range can be tuned by variation of hydrogen and also oxygen content within the material. Variations of oxygen content in a-SiO_x:H films were reported to result in photon energy emission ranges as large as from 1.3 to 1.7 eV (Carius, 2000). The different ranges of PL emission due to several possible origins of PL are also summarized by Voigt et al.

4.1.2 Surface hydrides

Surface -SiH_2 species were found to be essential to the visible PL of AE-PSi (Tsai, 1991) and proposed as possible origin of PL of AE-PSi (Wolford, 1983). However, this hypothesis in the course of research was falsified. Main knock-out criterion were observations by FTIR studies, which showed that PL can be quenched for AE-PSi samples, while only a small fraction of surface hydrides is removed from the sample by thermal desorption, but the main part of the hydrides still remain on the samples surface. Hence, there is "no direct correlation between the PL and the silicon hydrogen surface species" (Robinson, 1993). The passivation quality of the surface hydrides rather seem to imply a PL, and not the hydrides themselves are a source of PL. Similar PL can be obtained by AE-PSi either passivated by hydrides – as it is known to naturally be the case for freshly prepared samples – or passivated by a high quality surface oxide. Also, recently methoxy (-OCH_3) group passivation of the surfaces of porous silicon appear to have a similar passivation effect as hydrides or well grown oxygen. In summary, surface hydrides have been shown not to be direct source of the main part of visible PL in AE-PSi.

4.1.3 Defects

Several possibilities of carrier location at distortions of stoichiometrically built crystal lattices can be accounted to the category of defects. These defects can be either localized within the c-Si cores of AE-PSi, or are found near the boundaries of the crystalline cores within the AE-PSi samples. Near the oxide of the c-Si cores, defects are formed more often, because only there the elemental ratios show up gradients, dependent on the surface treatment of the samples after preparation. For the case of oxidized samples the material composition shows a transit from c-Si to SiO_2, where one has to keep in mind that additionally hydrogen can be incorporated due to initial hydrogen termination of the surfaces immediately after preparation. Known defects of this kind are three types of non bridging oxygen centers (NBOCs). These defects consist in trapped holes located at an oxygen atom owing a bond only to one neighbour atom. The first kind of this defect is an "isolated" Si-O, the second one is stabilized with a hydrogen bond Si-O … H-O, the third type is the least understood and is likely to be caused by the strain of bonding configurations or density (Prokes, 1996). NBOCs emit light in with peaks around 1.9 eV and FWHM of 0.1 to 0.3 eV – depending on which types of the various forms of NBOCs are present in the material (Skuja, 1979; Hibino, 1985; Munekuni, 1990; Nishikawa, 1991).

Most important support for the relevance of defect states in the luminescence of AE-PSi was derived from electron spin resonance (ESR) measurements. We therefore introduce the relevant ESR specific nomenclature, following (Prokes, 1996), see Fig. 10: Oxygen shallow donors (SDs) have been described as oxygen clusters at a silicon vacancy, in AE-PSi they occur near the sample surfaces and consist of a cluster of NBOCs. Furthermore, dangling bonds exist at silicon surfaces, if they are not entirely passivated by hydrogen or other species; they are called P_b centres in ESR nomenclature. After oxidation of freshly prepared AE-PSi a new type of defect appears in ESR measurements, called EX center. According to Stesmans et al. (Stesmans, 1994) EX centers consist of NBOC clusters, sharing a delocalised electron. These three types of Si-O related defect centres are suggestively sketched in Fig. 3. A major pro argument for the hypothesis that defects play a considerable role in the PL of AE-PSi was the observation that at low temperature annealing the P_b signal increased together with the SD signal and at the same time PL became more intense (Prokes, 1996). This experimental result cannot be explained by the non-radiative recombination channel,

which is opened by P_b centers, because PL would have to decrease with increasing P_b signal. Thus, the variation in PL intensity is not controlled solely by a change in surface passivation, but must have other reasons. An evident explanation is that the increase of SD signal – and therefore an increase in NBOC density - accounts for the higher PL yield.

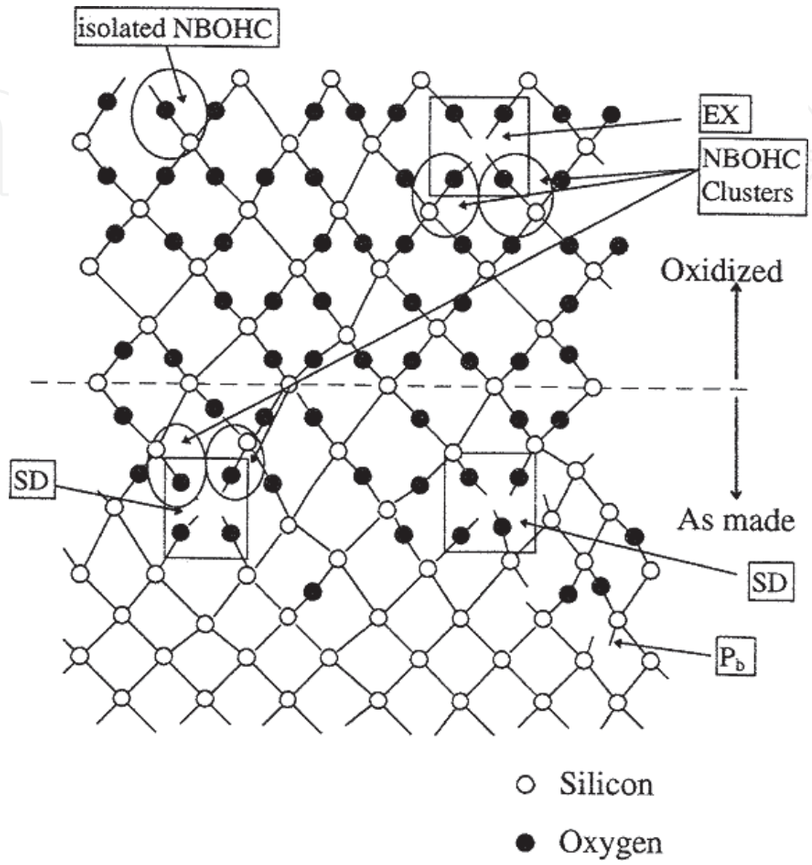

Fig. 10. Detailed model sketch of Si-O based NBOC defects; Reprinted with permission from (Prokes, 1995). Copyright 1995, American Institute of Physics.

A more elaborate model of how defects in the silicon oxide/silicon interface could act as luminescent centers within porous material Was discussed by Sacilotti et al. in (Sacilotti, 1993). It is based on the idea of type II semiconductor interface PL, which was inspired from the case of a AlAs/GaAlAs/AlAs heterostructure.

At this point we clearly state that different sources of PL can be present in differently prepared and differently surface treated AE-PSi. Further, the author believes that this point of view is helpful in understanding the PL of AE-PSi and of other kind of nanostructured silicon derivates, because there probably are a variety of existing PL mechanisms in complicatedly micro and nanostructured samples, and it is only a matter of knowing which PL channel prevails in each case, to appropriately explain the main PL mechanism.

4.1.4 Surface states

Reason for the presumption that surface states may play a role in PL of porous silicon structures was the consideration that the internal surface of porous silicon is very large.

There have been proposed 2 types of surface states for AE-PSi, one being energetically deep states, the other one shallow states (see Fig. 9d). Experimental evidence for the existence of non-quantum-confined states consisted in the observation of a large energy difference between absorption and PL peak in samples of AE-PSi (Lockwood, 1994). This energy difference was attributed to the existence of surface states, in which excited carriers relax after being absorbed in the crystalline parts of the material.

4.2 Photoluminescence in metal assisted wet chemically etched silicon

4.2.1 Introduction

Our main interest in PL on MAWCE-II silicon nanowire (SiNW) structures is to explore the origin of PL in each material produced with specific preparation parameters, which is a scientific basic research concern. In addition, the view on application of such obtained classes of materials is very challenging. As it is said in the credo of the semiconductor industry that "if it can be done in silicon, it will be done in silicon" (Vetterl, 2000), also light emitting devices will be built from silicon if sufficiently strong and fast emitters will be feasible. It's this respect, which the applied side of development aims to building a "silicon diode" or even better, constructing a "silicon laser". In this respect it is essential to overcome two main shortcomings of bulk c-Si.

A The band gap in the infrared regime of the spectrum
B The long PL lifetimes, which are related to the indirect nature of the silicon band gap

Shortcoming A was already solved by emission of visible PL of AE-PSi and this feature is still maintained by the material obtained by MAWCE-II. Shortcoming B is more complicated to be eliminated. Many approaches have been followed so far, but the final goal has not been reached yet, as one can see from the observation that no "silicon laser" with silicon or silicon compounds as active part of the device is available on the market to the best of the author's knowledge. Nevertheless, silicon based light emitting devices (LEDs) with c-Si as the light emitting source already exist in laboratories. Green et al. (Green, 2001) introduced a c-Si based device, similar to a high efficiency solar cell, but this LED emits in the infrared region with photon energies near 1.1 eV and therefore does not overcome drawback A. Presti et al. (Presti, 2006) published an article about electroluminescence of a Si quantum dot based LED in combination with a photonic crystal structure. This device emits light in the visible range of the spectrum, however to the best of the author's knowledge, they are not available on the market. And devices based on silicon nanocrystals (Si-NCs) do – as far as the author knows – not overcome drawback B. In Si nanocrystals the nature of the band gap is still predominantly indirect (Guillois, 2004). This issue is especially important, because long radiative lifetimes imply low emission decay rates, lead to low quantum yields at high excitation and finally hinder the design of a Si laser.
Solar cells built from AE-PSi or material produced by MAWCE follow a similar track, with the difference that shortcoming B is not so relevant in this case. For solar cells, the desired output is electric energy and not radiative emission. The negative nature of B for solar cells is only that absorption for indirect band gap semiconductors is very low as compared to direct band gap semiconductors.

4.2.2 Samples prepared from heavily doped and from weakly doped c-Si wafers

Fascinating feature of samples prepared from heavily doped wafers by MAWCE-II is their shiny bright visible PL emitted in the orange-red spectral range (Fig. 11b). This strong

visible light emission is only observed for samples prepared from heavily doped silicon wafers (by about 10^{20} cm^{-3}), whereas samples from weakly doped wafers (about 10^{16} cm^{-3}) show considerably weaker light emission (see Fig. 13). We observed that this trend does not, or only marginally, depend on the type of doping, on whether it is n-type or p-type. All PL measurements presented in this section were performed on a setup as described in our previous work (Sivakov, Voigt, 2010).

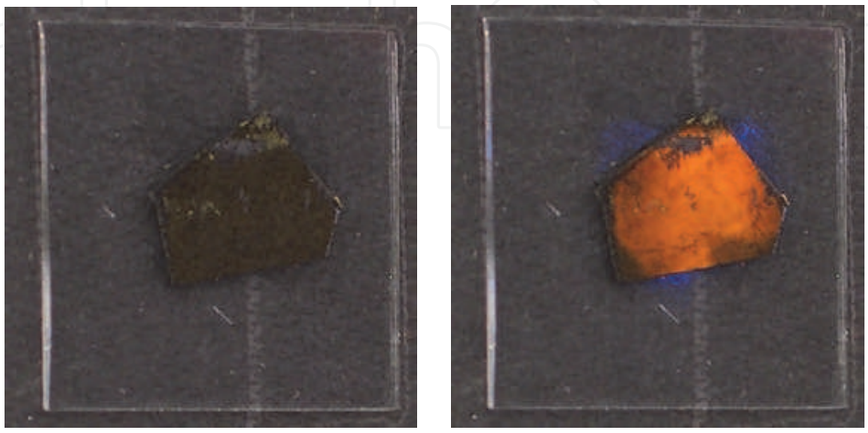

(a) (b)

Fig. 11. Bright visible orange-red PL as seen from a heavily doped sample prepared by MAWCE-II. (a) Sample as seen under exposure to white light; (b) the same sample additionally irradiated by laser light at wavelength of 337 nm. Blue luminescence is due to the glass substrate whereon sample was mounted. Reprinted from (Voigt, 2011).

Complementarily, structural investigations by SEM have shown that MAWCE-II samples prepared from heavily doped wafers own a mainly porous nanostructure (see Fig. 12a), whereas samples prepared from weakly doped wafers for certain preparation conditions are composed of SiNWs standing on the substrate like grass on an English yard's garden (conf. Fig. 2c). If one looks at the porous-like structure of the heavily doped samples in more detail, one observes that they also show up longish, wire-like features (Fig. 12b). These features might, however, not be of crystalline type, but again porous themselves as we observed in TEM measurements (not shown in this publication) and as (Qu, 2009) also pointed out for similarly prepared samples.

As the strong visible PL of the porous-like, heavily doped MAWCE-II samples reminds of the PL observed from high porosity AE-PSi – obtained by heavily doped, but non-degenerate p-type wafer material (Lehmann, 1991) – this implies that the nanostructure of the MAWCE-II samples might be very similar to the on of highly porous AE-PSi samples. In comparison to AE-PSi samples, we conclude that

- the large PL yield of heavily doped MAWCE-II samples in the visible range reminds of similar PL observed for highly porous AE-PSi.
- the microstructure of weakly doped MAWCE-II samples shows up SiNWs, in best case similar to Fig. 2c.
- the microstructure of heavily doped MAWCE-II samples resembles that of highly porous AE-PSi, with the difference that in highly doped MAWCE-II samples also wire-like structures are seen, but these are probably porous themselves again.

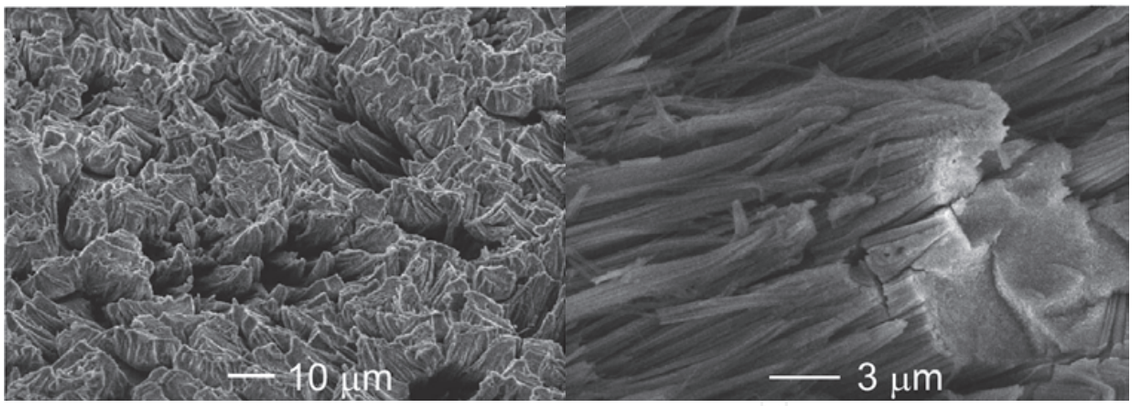

(a) (b)

Fig. 12. SEM microstructure studies of heavily doped (10^{20} cm^{-3}) MAWCE-II silicon surfaces (Voigt, 2011). (a) Unordered, porous-like structure seen in top view; (b) in side view and larger magnification it becomes visible that also in this material wire-like features are present.

One has to bear in mind that as well by anodic etching as by MAWCE-II a large variety of microstructures can be achieved, sensitively depending on the initial wafer type and the following etching conditions. With this respect it is illustrative to especially examine the overall influence of the initial wafer's doping density on the nanostructure and the PL spectra. Fig. 13 shows PL spectra, which where obtained from various samples, prepared by MAWCE-II.

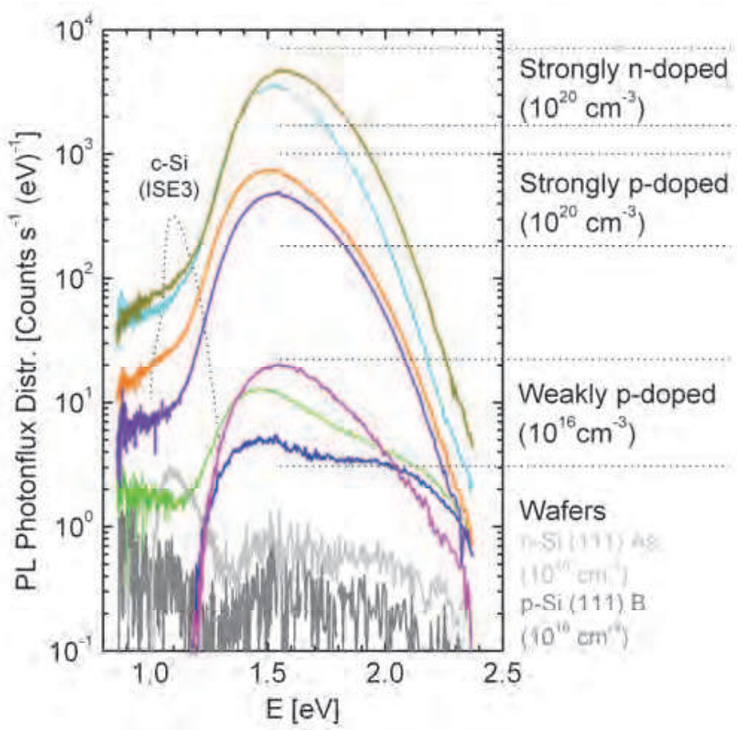

Fig. 13. PL spectra of differently doped as-prepared, oxidized samples, prepared by MAWCE-II. Dotted line and solid grey lines denote PL of crystalline Si wafers, showed for comparison.

Main trends in the yield of the different samples can be related to the initial wafers' different grades of doping. The higher the doping density is, the higher quantum PL yield will be gained. It became evident from more extensive measurement series that for MAWCE prepared samples this relation holds, independently whether n-type or p-type initial wafers are used (not shown in this publication). The type of doping plays a minor role and does not disturb the main general trend. Additionally, we performed measurements of PL spectra after an etch in dilute HF (dashed lines), which will be treated in the following subsection.

4.2.3 Influence of subsequent HF treatment to MAWCE samples

What is interesting in the observation of PL prior and posterior to HF treatment of the already oxidized MAWCE produced samples, is the ability to distinguish between PL sources, which are due to the oxide-free part of the sample and sources which lie in the oxide or the oxide/silicon interface. This is possible because an etch in dilute HF strips off the oxide from the sample and after removal from the etchant the surface of the nanowire-like or porous material is still passivated by hydrogen atoms (Ikeda, 1995; Kolasinski, 2009). According to our experience this passivation sufficiently holds for duration of about 5 to 10 min, in order not to perturb spectral PL measurements. Fig. 14a shows measurements of PL before and after etching in diluted HF (2.5%) for duration of 3 min. After the HF bath, the samples were rinsed by deionized (DI) water and blown dry by ambient air. The sample under investigation for re-oxidation investigations (Fig. 14b) was prepared from an n-type c-Si (111) wafer, doped by arsenic As with a density of 10^{20} cm^{-3}. It was prepared by a MAWCE-II process and is of highly porous type rather than nanowire containing. One clearly sees that

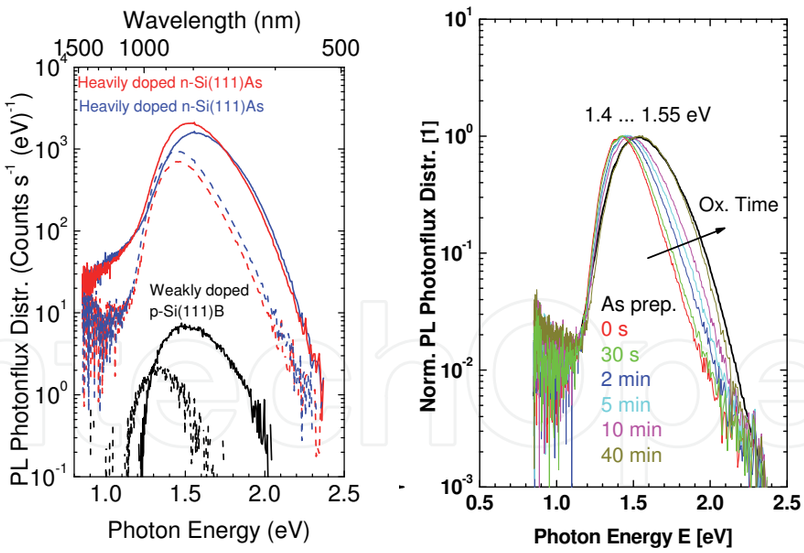

(a) (b)

Fig. 14. Spectrally resolved PL of samples prepared by MAWCE (Sivakov, Voigt 2010). (a) PL measurements before (solid line) and after (dashed line) HF treatment on the as-prepared, already oxidized samples of different doping; (b) re-oxidation of an HF treated porous sample. All curves are normalized to obtain the value 1 in the maximum. Also indicated is the PL measurement on the as prepared, oxidized sample. Oxidization times after the first measurement are listed in the legend.

PL of all samples shrinks by the HF treatment and the peak shifts from higher to lower photon energies (Fig. 14a). We attribute this to a loss in energy states, which were due to the silicon oxide film or the Si/SiO_x interface. These hypothetic energy states must be located in high energy range with photon energies around 1.6 eV, whereas the remaining PL is centred around 1.4 eV. The remainder of PL at all after etching is a strong hint to the existence of quantum confined states within the material. Quantum confined states giving rise to a PL emission with peak at 1.4 eV can be attributed to silicon nanocrystals with mean diameter of approximately 6 nm, if one follows the equation

$$\frac{d}{\text{nm}} = \left(\frac{3.73 \text{ eV}}{E_{PL} - E_{g,Si}} \right)^{1/1.39} \tag{12}$$

where d, E_{PL}, $E_{g,c\text{-}Si}$ = 1.12 eV mean the nanocrystal diameter, PL peak energy and silicon RT band gap, respectively. Eq. 12 can be derived by simple reorganization of formulae given in (Delerue, 1993) and (Ledoux, 2000).

4.2.4 Re-oxidization of HF treated sample

By observation of the re-oxidation of HF treated samples, further insight in the PL mechanism and sources of PL is gained. The advantage of measurements during reoxidation as compared to the previously discussed observation of the effect of HF treatment is that a process is monitored and not only initial and final states are observed. Normalized PL spectra, recorded during this process are shown in Fig. 14b. The black line designates the as-prepared, oxidized sample. After removing the sample from the HF etchant, rinsing it by DI water and blowing it dry by air, we had to wait for < 3 min until the first PL measurement could be performed, for transfer and sample mounting reasons. The measurement performed directly after this time is labelled by "0 s". We assume that no or very little effect of re-oxidation in ambient air happens during the transfer time. The results show that the initial state of the as-prepared sample was nearly reached after 40 min of re-oxidation.

4.2.5 Models

Various models have been proposed in order to describe PL arising from AE-PSi; examples have been enumerated and explained in Section 4.1. Here, we want do discuss in more detail about models appropriate to explain the main features observed during RT PL experiments on MAWCE-II prepared samples, as described in Sections 4.2.1 to 4.2.7.

2-media model comprising localized confinement

We start with a simple 2-media model sketched in Fig. 15a, which can be applied to SiNW containing samples of this kind. The black "stalk" in the middle of Figs. 15a and b symbolizes the crystalline core of the nanowire. Small nanocrystals are located within the SiO_x layer surrounding the SiNW. They are isolated from each other and from the SiNW stalk by SiO_x. As the PL contribution due to the crystalline SiNWs can be neglected if their diameters are large enough, main parts of the PL spectrum will stem either from quantum confined states or SiO_x-related states. Because of the assumption of only 2 PL active sources within the material, we call the model a 2-media model. PL from the medium of Si-NCs in this model corresponds to light emission from quantum confined states. PL from the

medium of SiO_x can be attributed to amorphous SiO_x (see Subsec. 4.1.1 and Carius, 2000), to Si-O related defects (see Subsec. 4.1.3) or to surface states localized at the Si/SiO_x boundary (see Subsec. 4.1.4).

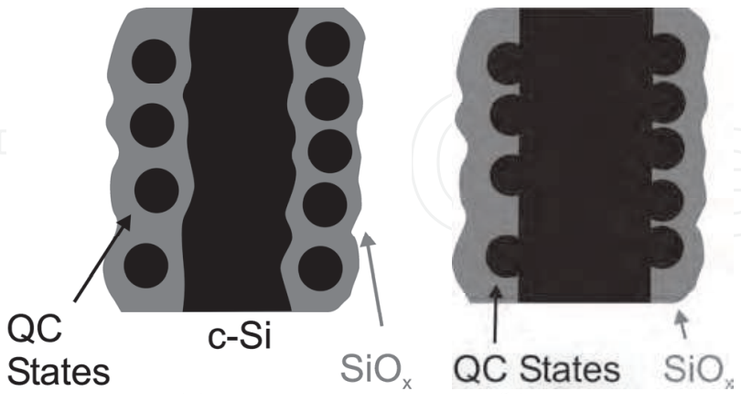

Fig. 15. Two-media models for SiNWs containing samples prepared by MAWCE. The dark part in the middle of the figures symbolizes a single crystalline SiNW. (a) Model of localized confinement of charge carriers in isolated Si-NCs within a matrix of amorphous SiO_x. (b) Model of semilocalized confinement of charge carriers within Si-NCs, being still attached to the crystalline core of a SiNW.

"Millet gruel" model

The 2-media model of localized confinement shown in Fig. 15a can account for PL measurements on MAWCE-II silicon, which really show crystalline-core SiNWs within the material. However, under certain deposition conditions no SiNWs are found inside the etched part of the wafer and another model has to be considered. For some MAWCE-II silicon a model holds, which we call the "millet gruel" model. The millet seeds within the gruel symbolize the Si-NCs within the porous matrix and the milk-starch-mixture surrounding the seeds symbolizes the oxide layers (see Fig. 16). Although there are no wire-like or more extended structures present within the millet gruel, it looks similar to a SEM

Fig. 16. The "millet gruel" model of porous silicon. It can be appropriate for AE-PSi as well as for MAWCE samples, while strongly depending on preparation parameters. The millet seeds symbolize single silicon nanocrystals, which are interconnected by milk-starch-mixture mush, symbolizing the SiO_x regions of porous Si.

micrograph of AE-PSi, shown in Fig. 12a. Also in the millet gruel wire-like features are formed, but they do not consist in longish seeds, but in seeds bonded together by an adhesive medium. Likewise, in highly porous AE-Psi as in samples belonging to Fig. 12a there may not be any SiNWs present and the longish structure to be seen in the figure might only be a chain of Si-NCs glued together by SiO_x. In this case, and only in this case, the "millet gruel" model is appropriate. In comparison to the 2-media model of localized confinement, this model only lacks the interface between the crystalline SiNWs and the SiO_x, and the SiNW cores themselves.

2-media model comprising semi-localized confinement

The 2-media model comprising semi-localized confinement resembles the one assuming localized confinement. In both cases crystalline SiNWs are present within the regarded material. The only difference between the models is that in the semi-localized case the Si-NCs are still attached to the crystalline SiNW core, forming kind of protuberances at a rough Si-NW surface. Actually, by TEM investigations, SiNWs with very rough surfaces have been found in weakly doped MAWCE-II silicon (Sivakov, Voigt 2010). The corresponding peak to valley height of the sidewall roughness was found to lie in the range between 2.5 to 3.5 nm. In order to understand, how a shift of PL emission peak energies can be explained by the model of semi-localized confinement, one has to regard 3 items:

- Confinement within the Si-NC-like protuberances will only occur, if one of the two charge carriers – either the electron or the hole – is trapped at some surface part of the protuberance. Two quasi-freely existing charge carriers of opposite electrical charge, or more precisely an exciton, would not move into a protuberance, where the total energy will be increased due to quantum confinement.
- Several energy contributions have to be taken into account, if one wants to calculate the energy of the finally emitted photon. These are
  - the Coulomb-attraction between the electron and hole, $\mathbf{\Delta E_{Coul}}$
  - the energy decrease of the exciton due to localization of one charge carrier in a trap, $\mathbf{\Delta E_{trap}}$
  - the energy increase of the system due to (semi)confinement, $\mathbf{\Delta E_{conf}}$
- The state achieved as semi-localized state (one carrier trapped at surface of protuberance) must be of stable or metastable type. I.e., an energy barrier must exist for the electron hole pair to diffuse into the bulk of the SiNW and form a free (if the SiNW diameter is large) or a wire-confined state (if the SiNW diameter is small).

In summary, the energy $\mathbf{E_{Phot}}$ of the emitted photon can be calculated as

$$E_{Phot} = E_g + \Delta E_{conf} - \Delta E_{Coul} - \Delta E_{trap} \pm E_{Phon}\,, \tag{13}$$

where $\mathbf{E_g}$, and $\mathbf{E_{Phon}}$ denote the semiconductor band gap and the energy of an emitted or absorbed phonon.

A similar model as the one of semi-localized confinement has already been proposed to explain the process of electroluminescence (EL) generation of AE-PSi by (Billat, 1996). The latter model is sketched in Fig. 17. Additionally to the kind of "semi-localized Si-NCs" to be seen at the boundary region of the material, the model does also incorporate the development of the material's surface structure by the process of electrochemical oxidation within the electrolytic environment during the EL emission (oxidation process steps in Figs. 17a-c). The proposed oxidation leads to a decrease of the Si-NC like structures'

diameters, which is in accord with the observation of a shift of the PL peak to higher photon emission energies with time. As higher photon energies correspond to lower diameters in the framework of quantum confinement models, the observation of shift together with the proposed model are strongly supporting the hypothesis of the possibility of semi-localized quantum confinement within Si-NC-like protuberance.

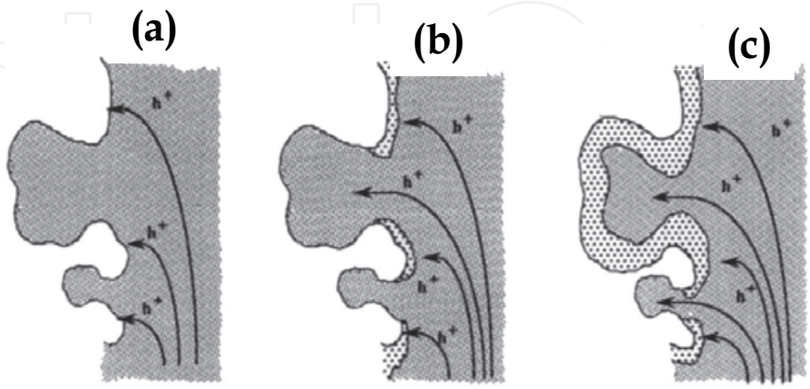

Fig. 17. Sketches of a model designed to explain the electroluminescence (EL) of AE-PSi. Image from (Billat, 1996). Reproduced by permission of ECS – The Electrochemical Society. Single Si-NC-like protuberances are seen at the boundary of the bulk Si part. Steps (a), (b), (c) symbolize the evolution of the material due to oxidation in electrolytic environment during EL measurements.

Model of self-trapped exciton (STE)

The model of semi-localized confinement can be complemented by the model of self-trapped excitons (STEs), described by Delerue et al. (Delerue, 2004 in Sec. 6.4). In the latter model it is assumed that under certain circumstances an electron hole-pair can be localized on a single covalent bond. If the implicated lattice displacements of the two corresponding atoms are large enough, the separation between the anti-bonding and the bonding state will decrease much, leading to a large energy shift between the photon absorption in the bulk part and the photon emission, due to the exciton localized on the bond (Stokes-shift). A large Stokes-shift of about 1 eV has actually been observed for a sample of oxidized AE-PSi with crystallite diameters of about 1.5 nm (Lockwood, 1994), as was already mentioned in Subsec. 4.1.4, dealing about surface states. The model of STEs was accompanied by calculations of various kind (Delerue, 2004), hence it can be regarded as theoretically funded.

4.3 Discussion and conclusions

We focused on spectral RT measurements of PL on MAWCE-II silicon in this section, including investigations on

1. the dependence of spectral PL on doping grade of the samples,
2. surface treatment by HF and
3. re-creation of PL due to reoxidation.

Samples can be either of SiNW-like type – corresponding to weakly doped initial wafers – or of porous type, resembling AE-PSi – corresponding to heavily doped initial wafers. SiNW-like samples usually show up low PL emission, whereas samples of porous types emit

strong visible PL in the red-orange spectral range. After treatment by dilute HF the high-energy part of PL vanishes – as well for SiNW-like as for porous samples. Interestingly the disappearance takes place not in the total spectral range, but significant PL contributions remain centred around the peak energy at about 1.4 eV. We conclude that different sources of PL are present in the MAWCE-II processed samples. This is evident from PL measurements before and after HF treatment of the as-prepared, already oxidized samples and from the process of re-oxidation. We explain these observations by the following models, which categorize different parts of the PL spectrum to different structural features or regions, corresponding to the sources of PL as discussed for AE-PSi in Subsec. 4.1.

i. The 2-media model of **localized** Si-NCs within a matrix of SiO_x surrounding the SiNWs in MAWCE-prepared samples (Fig. 15a) sufficiently explains the origin of PL prior and posterior to HF treatment. The crystalline silicon core of the nanowires plays with respect to PL emission no role, hence this model can also be applied to highly porous structures, where only Si-NC-like features are present embedded in an amorphous matrix of SiO_x. In this regard the 2-media model of localized confinement can for highly porous samples better be changed to the "millet gruel" model (see Fig. 16). By means of this model also the development of PL after HF etching and during the process of re-oxidation can be interpreted. After the HF etch, the oxide around the Si-NCs and the SiNW is entirely removed. Therefore only PL from quantum confined states within the Si-NCs remains (being centered at about 1.4 eV as seen in Fig. 15a, b). During the process of re-oxidation two processes occur simultaneously. Firstly, the SiO_x layer is built up again, leading to steadily increasing SiO_x-related PL. Secondly, the diameters of the Si-NCs shrink, which increases the confinement energy according to eq.12, hence the confinement part of the PL shifts to higher energies. The first process is readily seen in Fig. 4b, process 2 plays a minor role and its effect is only visible after application of successive HF etch steps.
ii. The **"millet gruel"** model is a submodel of the 2-media model of **localized** confinement, the only difference being the leave-out of the crystalline SiNW cores. This model applies for highly porous Si material.
iii. Another 2-media model featuring **semi-localized** Si-NCs within the matrix of SiO_x was introduced (Fig. 15b). It can explain PL emanating from SiNWs with rough surfaces, without assuming the existence of isolated Si-NCs within the SiO_x matrix. However, this model currently lacks direct experimental support and theoretical foundation and is therefore speculative.

another model was cited in Subsec. 4.2.5, which explains the PL of porous Si with very small diameters around 1.5 nm as a result of self trapped excitons (STE), being localized at the boundary of small Si-NCs (see ref. Delerue, 2004). This model resembles the 2-media model of **semi-localized** confinement, but in contrast to semi-localized confinement, which was proposed to explain PL emission from rough surfaces of large-diamenter SiNWs, the STE model in silicon was applied to explain PL emission of very small diameter Si-NCs.

Surely, more detailed, more extended experimental PL investigations on the MAWCE-II silicon are sensible (as well as reviews on already published results). To name some of them:

- Time dependent PL measurements, like PL decay
- Temperature dependent PL
- PL excitation measurements

There are many other, especially micro-, and nano-scopic, experimental approaches, which either already exist or still have to be found, which can be applied to materials obtained by MAWCE-II and give further insight into PL mechanisms and responsible sources of photoluminescence. Especially, scanning optical near field (SNOM) measurements on single, isolated SiNWs produced by MAWCE–II or even more simple micro-PL measurements – can give insight and either verify or falsify the model of the PL by semi-localized Si-NCs within an SiO_x matrix (see Fig. 15b). In summary, the PL of MAWCE-II samples is a very exciting, buzzing field of investigation and it's likely that a lot of insights and relations still wait to be discovered.

5. Solar cell architectures based on wet chemically etched silicon nanowires

Among various sources of energy, sunlight is the most abundant and cleanest natural energy resource. In principle, photovoltaics (PVs) hold a great promise to exploit the sunlight to generate clean energy to accommodate the ever-increasing energy demands [Barnham, 2006; Crabtree, 2007; Alsema; 2000]. Photovoltaics is the field of technology and research related to the application of solar cells for energy generation by converting solar energy directly into electricity. Electrical production with solar cells is continuously increasing. Solar cells are particularly useful as power generators in distant and terrestrial places like weather stations and satellites. Solar cells are used in small devices like watches and calculators, but mostly they are used to produce electricity either in large-scale power plants or by being incorporated into walls and rooftops. The function of solar cells essentially involves the presence of a p-n junction close to its surface in order to create potential difference in the bulk. A transport of photogenerated charge carriers across the junction to lower its potential energy is harnessed to execute work. About 90% of solar photovoltaic modules are silicon-based [Miles, 2007], but in recent years increased demand for silicon solar cells has inflated the price of solar-grade silicon. The price of Si accounts for about half of the price of solar cells. The grid parity of electricity produced by solar cells is close to 1 USD/Watt assuming a 20-year lifetime of the cells [Gunawan, 2009], but the price is currently four times higher. One obvious way to lower the cost is to reduce the amount of silicon in the cells. By using thin film technology, the thickness of the silicon can be reduced from 200–300 μm to 0.2–5 μm. Another way to cut down production cost is to use low-grade Si instead of ultra-pure Si currently being used. However, this lower-grade material is less efficient. It is presumed that the grid parity of solar cells will be reached by using thin film technology or a new design that is most-likely based on nanotechnology.

5.1 Axial p-n junction in MAWCE SiNWs

Wet chemically etched microcrystalline silicon (mc-Si) surfaces show very low reflectance compared to Si thin layers or wafers [Stelzner, 2008; Andrä, 2007, 2008]. This low reflectance is potentially interesting for photovoltaic applications where enough absorption of solar light in an as thin as possible Si layer is desired and a combination of light trapping structures and antireflective coatings have usually to be applied [Tsakalakos, 2007; Peng, Xu, 2005]. The SiNWs themselves have shown to absorb solar light very satisfactorily and can therefore be used as the solar cell absorber [Tsakalakos, Balch, 2007; Kaynes, 2005; Koynov, 2006].

In this part we will show how the wet chemical etching into a thin silicon layer on glass substrate to be useful to serve a solar cell absorber in a thin film solar cell concept on glass. Fig. 18 shows a schematic representation of the multicrystalline silicon layer stack on glass before wet chemical etching. Fig. 19 shows scanning electron microscopy (SEM) micrographs of the SiNWs after wet chemical etching into the mc-Si layers on glass. Fig. 19a shows an SEM micrograph of SiNWs in cross section. The etching profile is homogeneous and the etching depth approximately is 2 μm from the top surface. Fig. 19b shows a SEM micrograph of SiNWs from the top surface. A difference in the SiNW orientation is discernible for starting grains of different orientation prior to wet chemical etching. The diameter of the SiNWs varies from 50 nm to 150 nm with an average of approximately 100 nm.

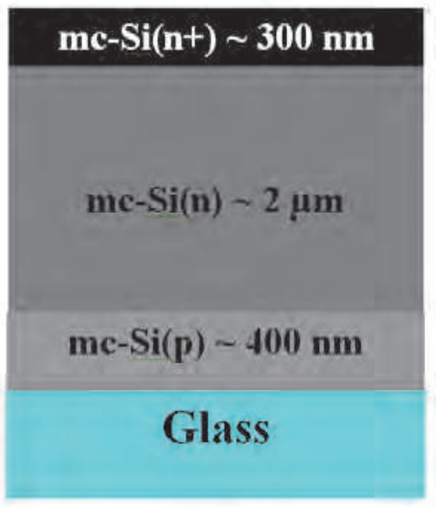

Fig. 18. Schematic cross sectional view of the mc-Si p-n junction layer stack on a glass substrate.

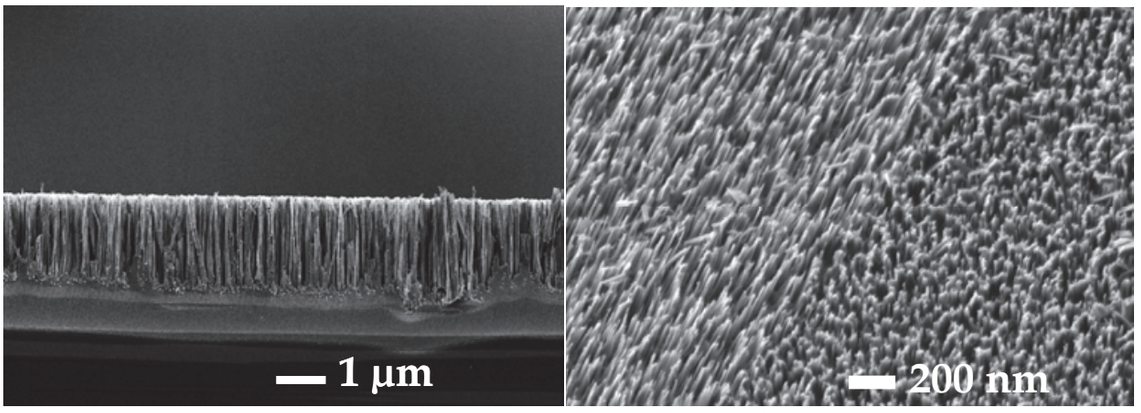

(a) (b)

Fig. 19. (a) Cross sectional SEM micrograph of the $AgNO_3$/HF etched mc-Si layer on glass; (b) planar SEM micrograph of SiNWs etched into grains of different orientation; the grain boundary in the staring mc-Si layer is clearly discernible (Sivakov, 2009).

SiNWs have been contacted by metallic tips for the characterization of the optoelectronic properties. The samples were illuminated through the glass substrate (superstrate configuration) using well defined AM1.5 illumination conditions. I-V-curves are shown in Fig. 20. The four different curves were obtained at four positions within a single sample. While in all cases the open circuit voltage (V_{oc}) is rather similar lying in the range of 410 - 450 mV, the short circuit current (I_{sc}) values differ appreciably. This may be due to the point contacting with gold needles which allows either to contact a higher or lower number of SiNWs just depending on position. Therefore, it is not simple to give a reliable current density. The short circuit current densities, j_{sc}, in Fig. 20 ranging from 13.4 mA/cm² to 40.3 mA/cm² were calculated. The shunting is responsible for the deviation of the I-V-curve parallel to the y-axis; a large series resistance is responsible for a deviation of the curve parallel to the x-axis. Shunting may be due to the large unpassivated surface of the SiNWs or even due to surface currents along the SiNW surfaces. High series resistance and shunting lead to a low fill factor FF of about 30%. From the measured values an energy conversion efficiency (η) of 1.7% to 4.4 % follows. The highest power conversion efficiency of SiNWs based solar cell on glass was 4.4 % which shows potential for low cost solar cells with such design. The high current density of about 40 mA/cm² requires complete light absorption and high quantum efficiency. Moreover, to increase the power conversion efficiency for such nanostructures, the shunting should be minimized and all production steps must be optimized for such solar cell architecture.

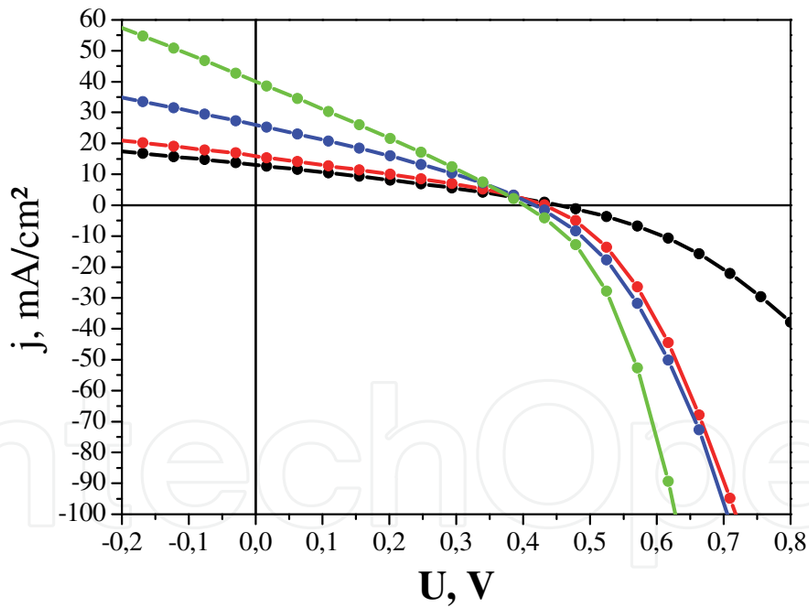

Fig. 20. Illuminated (AM1.5) I-V curves of SiNWs etched into a mc-Si layer on glass. SiNW are irradiated through the glass substrate (super-state configuration) and contacted by metal tips at four different sample positions (Sivakov, 2009).

5.2 n-SiNWs/Al_2O_3/AZO semiconductor-insulator-semiconductor isotype heterojunction

In this part we will present a semiconductor-insulator-semiconductor (SIS) concept based on very efficiently light absorbing wet-chemically etched SiNWs as presented in Fig. 21.

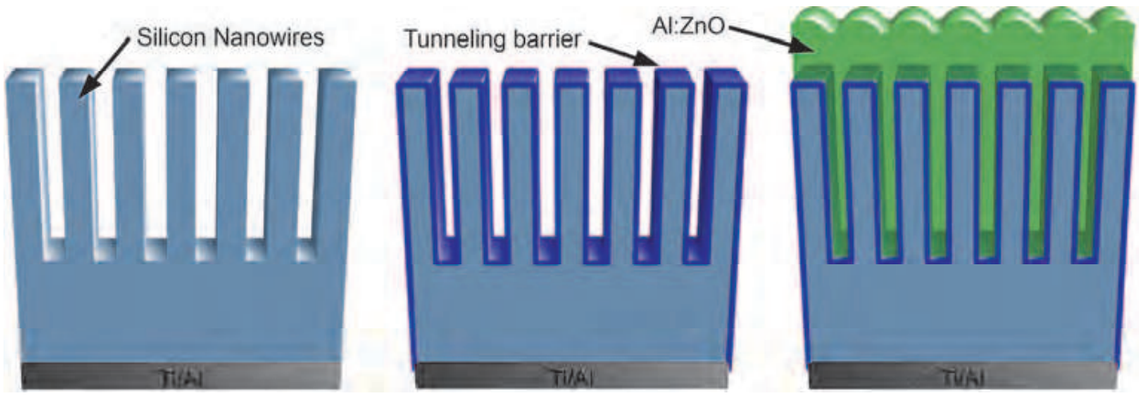

Fig. 21. Schematic cross sectional view of the formation of semiconductor-insulator-semiconductor solar cell based on wet chemically etched silicon nanowires.

Fig. 22 shows cross sectional SEM micrographs of the SiNWs after wet chemical etching of single crystalline n-Si(100) wafers and the same sample after atomic layer deposition (ALD) of alumina (Al_2O_3) as a tunnelling oxide and aluminium doped zinc oxide (AZO) as a front contact. The etching profile (Fig. 22a) is homogeneous and the etching depth is approximately 2 µm from the original wafer surface. Fig. 22b shows the homogeneous filling of the gaps between the SiNWs with Al_2O_3/AZO.

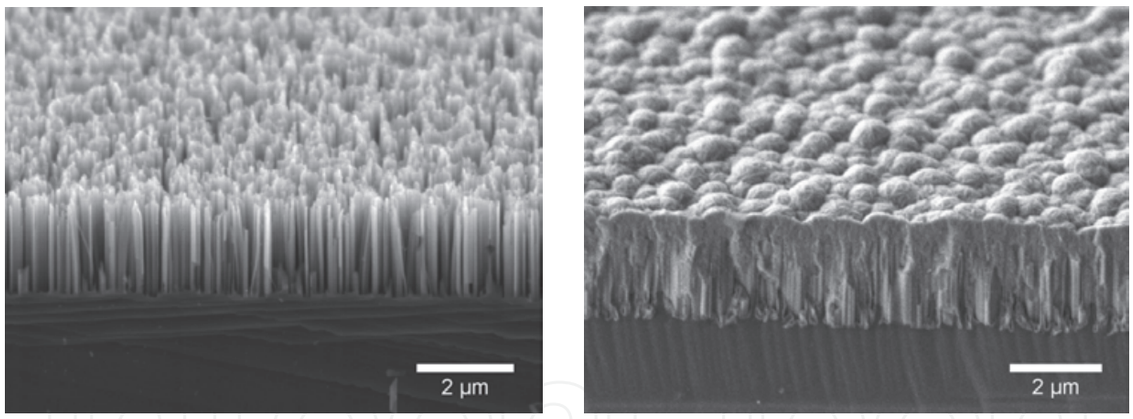

(a) (b)

Fig. 22. Cross sectional SEM micrographs of (a) as prepared wet chemically etched SiNWs; (b) the complete layer stack of an SIS solar cell with Al_2O_3 wrapped insulating as well as wrapped AZO films.

Illuminated and dark I-V-curves are shown in Fig. 23. The highest observed open current voltage ($V_{OC,\ max}$), short current density ($J_{SC,\ max}$) and fill factor (FF) under AM1.5 (1000W/m²) illumination were 470 mV, 33 mA/cm² and 61%, respectively. The solar cell with the best 8.6% efficiency is shown in Fig. 23.

In conclusion we have demonstrated a semiconductor-insulator-semiconductor (SIS) solar cell based on wet chemically etched silicon nanowires (SiNWs) and aluminium oxide (Al_2O_3) as a tunnelling barrier grown by atomic layer deposition (ALD). The highest power

conversion efficiency of SiNWs based SIS solar cell was 8.6 % which shows potential for low cost solar cells with such a design. The most promising and important factor is the improvement of the V_{oc} which can be tuned by the SiNW dominated surface structure. We see a real potential for further improvement of solar cell parameters such as V_{oc} to 600-700 mV and a power conversation efficiency of >15%.

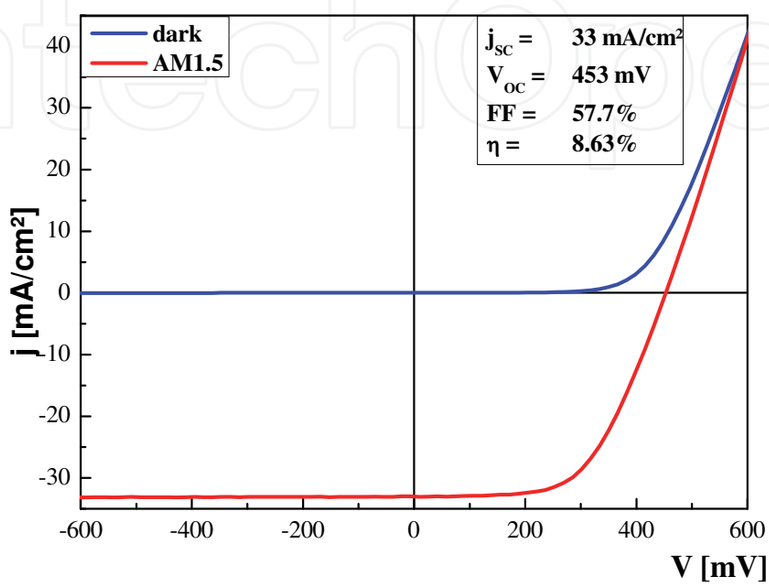

Fig. 23. Non illuminated and illuminated (AM1.5) I-V curves of an SIS solar cell with a 11 Å Al_2O_3 tunneling barrier layer and optimized SiNW structure. The SIS cell is contacted by metal tips, one on the rear wafer surface which is contacted by a Ti/Al layer and one on the front AZO layer surface.

6. Acknowledgments

The authors are gratefully acknowledged to Mr. H. Köbe and Mrs. A. Dellith (Institute of Photonic Technology, Jena/Germany) for the scanning electron microscopy investigations and to Mrs. S. Hopfe (Max-Planck-Institute of Microstructure Physics, Halle/Germany) for the preparation of the TEM samples. Prof. Gottfried H. Bauer is acknowledged for his great help by discussing the model of semi-localized quantum confinement. The authors gratefully acknowledge financial support by European Commission in part the European Project in the framework of FP7, "ROD-SOL" as well as by the Max Planck Society in the framework of the "NANOSTRESS" project.

7. References

[Allen, 2008] J.E. Allen, E.R. Hemesath, D.E. Perea, J.L. Lensch-Falk, Z.Y. Li, F. Yin, M.H. Gass, P. Wang, A.L. Bleloch, R.E. Palmer, L.J. Lauhon. High-resolution detection of Au catalyst atoms in Si nanowires. N*ature Nanotechnology* 3, 168 - 73 (2008).

[Alsema, 2000] E.A. Alsema. Energy pay-back time and CO_2 emissions of PV systems. *Prog. Photovoltaics* 8, 17 – 25 (2000).

[Andrä, 2007] G. Andrä, M. Pietsch, Th. Stelzner, F. Falk, S.H. Christiansen, A. Scheffel, S. Grimm. Proceedings 22nd European Photovoltaic Solar Energy Conference and Exhibition, Milan, Italy, September 3–7, 481 (2007).

[Andrä, 2008] G. Andrä, M. Pietsch, V. Sivakov, Th. Stelzner, A. Gawlik, S. Christiansen, F. Falk, Proceedings 23nd European Photovoltaic Solar Energy Conference and Exhibition, Valencia, Spain, September 1–5, 163 (2008).

[Barnham, 2006] K.W.J. Barnham, M. Mazzer, B. Clive. Resolving the energy crisis: nuclear or photovoltaics? *Nature Materials* 5, 161 - 64 (2006).

[Billat, 1996] S. Billat. Electroluminescence of heavily doped p-type porous silicon under electrochemical oxidation in galvanostatic regime. *J. Electrochem. Soc.* 143, 1055 – 61 (1996).

[Canham, 1990] L.T. Canham. Silicon quantum wire array fabrication by electrochemical and chemical dissolution of wafers. *Appl. Phys. Lett*. 57, 1046 (1990).

[Carius, 2000] R. Carius. Optical gap and photoluminescence properties of amorphous silicon alloys. *Philos. Mag*. B 80, 741–53 (2000).

[Civale, 2004] Y. Civale, L.K. Nanver, P. Hadley, E.J.G. Goudena. Aspects of silicon nanowire synthesis by aluminum-catalyzed vapor-liquid-solid mechanism. Proceedings of 7th Annual Workshop on Semiconductor Advances for Future Electronics (SAFE 2004), November 25-26, 2004, Veldhoven, The Netherlands, Publ. STW, ISBN 90-73461-43-X, 692-96 (2004).

[Chen, 2008] C.-Y. Chen, C.-S. Wu, C.-J. Chou, T.-J. Yen. Morphological control of single-crystalline silicon nanowire arrays near room temperature. *Adv. Mater*. 20, 3811 - 15 (2008).

[Crabtree, 2007] G.W. Crabtree, N. S. Lewis. Solar energy conversion. *Phys. Today* 60, 37 - 42 (2007).

[Cui, 2001] Y. Cui, L.J. Lauhon, M.S. Gudiksen, J. Wang, C.M. Lieber. Diameter-controlled synthesis of single crystal silicon nanowires. *Appl. Phys. Lett.* 78, 2214 (2001).

[Cullis, 1991] A.G. Cullis, L.T. Canham. Visible light emission due to quantum size effects in highly porous crystalline silicon. *Nature* 353, 335 – 38 (1991).

[Cullis, 1997] A.G. Cullis, L.T. Canham, P.D.J. Calcott. The structural and luminescence properties of porous silicon. *J. Appl. Phys*. 82, 909 – 65 (1997).

[Delerue, 1993] C. Delerue, G. Allan, M. Lannoo. Theoretical aspects of the luminescence of porous silicon. *Phys. Rev. B* 48, 11024 (1993).

[Delerue, 2004] C. Delerue, M. Lannoo. Nanostructures : theory and modeling. Berlin - New York : Springer (2004).

[Duan, 2001] X. Duan, Y. Huang, Y. Cui, J. Wang, C.M. Lieber. Indium phosphide nanowires as building blocks for nanoscale electronic and optoelectronic devices. *Nature* 409, 66 – 69 (2001).

[Ehbrecht, 1995] M. Ehbrecht, H. Ferkel, V. V. Smirnov, O. M. Stelmakh, W. Zhang, F. Huisken. Laser-driven flow reactor as a cluster beam source. *Rev. Sci. Instrum.* 66, 3833 (1995).

[Eisenhawer, 2011] B. Eisenhawer, D. Zhang, R. Clavel, A. Berger, J. Michler and S. Christiansen. Growth of doped silicon nanowires by pulsed laser deposition and their analysis by electron beam induced current imaging. *Nanotechnology* 22, 075706 (2011).

[Fuhrmann, 2005] B. Fuhrmann, H.S. Leipner, H.-R. Höche, L. Schubert, P. Werner, U. Gösele. Ordered arrays of silicon nanowires produced by nanosphere lithography and molecular beam epitaxy. *Nano Letters* 5, 2524 - 27 (2005).

[Givargizov, 1975] E.I. Givargizov. Fundamental aspects of VLS growth. *J. Cryst. Growth* 31, 20 - 30 (1975).

[Green, 2001] M.A. Green, J. Zhao, A. Wang, P.J. Reece, M. Gal. Efficient silicon light-emitting diodes. *Nature* 412, 805 – 08 (2001).

[Guillois, 2004] O. Guillois, N. Herlin-Boime, C. Reynaud, G. Ledoux, F. Huisken. Photoluminescence decay dynamics of noninteracting silicon nanocrystals. *J. Appl. Phys*. 95, 3677 – 82 (2004).

[Gunawan , 2009] O. Gunawan, S. Guha. Characteristics of vapor–liquid–solid grown silicon nanowire solar cells. *Solar Energy Materials and Solar Cells* 93, 1388 - 93 (2009).

[Haber@Weiss, 1935] F. Haber, J. Weiss. The catalytic decomposition of hydrogen peroxide by iron salts. *Proc. Roy. Soc.*, 147A, 332 - 51 (1935).

[Hannon, 2006] J.B. Hannon, S. Kodambaka F.M. Ross, R.M. Tromp. The influence of the surface migration of gold on the growth of silicon nanowires. *Nature* 440, 69 - 71(2006).

[Hanrath, 2002] T. Hanrath, B.A. Korgel. Nucleation and growth of germanium nanowires seeded by organic monolayer-coated gold nanocrystals. *J. Am. Chem. Soc*. 124, 1424 - 29 (2002).

[Heath, 1993] J.R. Heath, F.K. LeGoues. A liquid solution synthesis of single crystal germanium quantum wires. *Chem. Phys. Lett*. 208, 263 - 68 (1993).

[Hibino, 1985] Y. Hibino, H. Hanafusa, S. Sakaguchi. Drawing condition dependences of optical absorption and photoluminescence in pure silica optical fibers. *Appl. Phys. Lett*. 47, 1157–59 (1985).

[Hochbaum, 2005] A.I. Hochbaum, R. Fan, R. He, P. Yang. Controlled growth of Si nanowire arrays for device integration. *Nano Letters* 5, 457 - 60 (2005).

[Hochbaum, 2008] A.I. Hochbaum, R. Chen, R. Diaz Delgado, W. Liang, E.C. Garnett, M. Najarian, A. Majumdar, P. Yang. Enhanced thermoelectric performance of rough silicon nanowires. *Nature* 451, 163 - 67 (2008).

[Hochbaum, 2009] A.I. Hochbaum, D. Gargas, Y. J. Hwang, P. Yang. Single crystalline mesoporous silicon nanowires. *Nano Letters* 9, 3550 - 54 (2009).

[Huang, 2008] Z. Huang, X. Zhang, M. Reiche, L. Liu, W. Lee, T. Shimizu, S. Senz, U. Gösele. Extended arrays of vertically aligned sub-10 nm diameter [100] Si nanowires by metal-assisted chemical etching. *Nano Letters* 8, 3046 – 51 (2008).

[Huisken, 2002] F. Huisken, G. Ledoux, O. Guillois, C. Reynaud. Light-emitting silicon nanocrystals from laser pyrolysis. *Adv. Mater.* 14, 1861 – 65 (2002).

[Ikeda, 1995] H. Ikeda, K. Hotta, T. Yamada, S. Zaima, H. Iwano, Y. Yasuda. Oxidation of H-terminated Si(100) surfaces studied by high-resolution electron-energy-loss spectroscopy. *J. Appl. Phys.* 77, 5125 (1995).

[Jellison@Modine, 1982] G. Jellison, F. Modine. Optical constants for silicon at 300 and 10 K determined from 1.64 to 4.73 eV by ellipsometry. *J. Appl. Phys*. 53, 3745 (1982).

[Kamins, 2001] T.I. Kamins, R.S. Williams, D.P. Basile, T. Hesjedal, J.S. Harris. Ti-catalyzed Si nanowires by chemical vapor deposition: microscopy and growth mechanisms. *J.* Appl. Phys. 89, 1008 (2001).

[Kayes, 2005] B.M. Kayes, N.S. Lewis, H.A. Atwater. Comparison of the device physics principles of planar and radial *p-n* junction nanorod solar cells. *J. Appl. Phys.* 97, 114302 (2005).

[Kelzenberg, 2008] M.D. Kelzenberg, D.B. Turner-Evans, B.M. Kayes, M.A. Filler, M.C. Putnam, N.S. Lewis, H.A. Atwater. Photovoltaic measurements in single-nanowire silicon solar cells. *Nano Letters* 8, 710 – 14 (2008).

[Koch, 1993] F. Koch, V. Petrova-Koch, T. Muschik, A. Nikolov, V. Gavrilenko. Some perspectives on the luminescence mechanism via surface-confined states of porous Si. Mat. Res. Soc. Symp. Proc. 283, 197 (1993).

[Kolasinski, 2009] K. W. Kolasinski. Etching of silicon in fluoride solutions. *Surface Science* 603, 1904-11 (2009).

[Koynov, 2006] S. Koynov, M.S. Brandt, M. Stutzmann. Black nonreflecting silicon surfaces for solar cells. *Appl. Phys. Lett*. 88, 203107 (2006).

[Lauhon, 2002] L.J. Lauhon, M.S. Gudiksen, D. Wang, C.M. Lieber. Epitaxial core–shell and core–multishell nanowire heterostructures. *Nature* 420, 57 -61 (2002).

[Ledoux, 2000] G. Ledoux, O. Guillois, D. Porterat, C. Reynaud, F. Huisken and B. Kohn, V. Paillard. Photoluminescence properties of silicon nanocrystals as a function of their size. *Phys. Rev. B* 62, 15942 (2000).

[Ledoux, 2002] G.Ledoux, J. Gong, and F. Huisken, O. Guillois and C. Reynaud. Photoluminescence of size separated silicon nanocrystals: Confirmation of quantum confinement. *Appl. Phys. Lett*. 80, 4834 – 36 (2002).

[Lehmann, 1991] V. Lehmann, U. Gösele. Porous silicon formation: a quantum wire effect. Appl. Phys. Lett. 58, 856 (1991).

[Lockwood, 1994] D. J. Lockwood. Optical-properties of porous silicon. Solid State Communications 92, 101 (1994).

[Lieber, 2003] C.M. Lieber. Nanoscale science and technology: Building a big future from small things. *MRS Bull*. 28, 486 - 91 (2003).

[Lifschitz@Slyozov, 1961] I.M. Lifschitz, V.V. Slyozov. The kinetics of precipitation from supersaturated solid solutions. *J. Phys. Chem. Solids* 19, 35 - 50 (1961).

[McIntosh, 1902] D. McIntosh. Inorganic Ferments. *J. Phys. Chem*. 6, 15 - 44 (1902).

[Miles, 2007] R.W. Miles, G. Zoppia, I. Forbes. Inorganic photovoltaic cells. *Materials Today* 10, 20 - 27 (2007).

[Munekuni, 1990] S. Munekuni, T. Yamanaka, Y. Shimogaichi, R. Tohmon, Y. Ohki, K. Nagasawa, Y. Hama. Various types of nonbridging oxygen hole center in high-purity silica glass. *J. Appl. Phys*. 68, 1212 (1990).

[Nishikawa, 1991] H. Nishikawa, R. Nakamura, K. Nagasawa, Y. Ohki, Y. Hama. Proceedings of the 3rd Internat. Conf. on Properties and Applications of Dielectric Materials Vol. 1-2, pp. 1032–35 (1991).

[Oh, 2008] S.H. Oh, K. van Benthem, S.I. Molina, A.Y. Borisevich, W. Luo, P. Werner, N.D. Zakharov, D. Kumar, S.T. Pantelides, S.J. Pennycook. Point defect configurations of supersaturated au atoms inside Si nanowires. *Nano Letters* 8, 1016 - 19 (2008).

[Ostwald, 1900] W. Ostwald. Über die vermeintliche Isomerie des roten und gelben Quecksilberoxyds und die Oberflächenspannung fester Körpe. *Z. Phys. Chem*. 34, 495 (1900).

[Peng, 2002] K.-Q. Peng, Y.-J. Yan, S.-P. Gao, J. Zhu. Synthesis of large-area silicon nanowire arrays via self assembling nanoelectrochemistry. *Adv. Mater*. 14, 1164 - 67 (2002).

[Peng, 2005] K. Peng, Y. Wu, H. Fang, X. Zhong, Y. Xu, J. Zhu. Uniform, Axial-orientation alignment of one- dimensional single-crystal silicon nanostructure arrays. *Angew. Chem. Int. Edn.* 44, 2797 – 2802 (2005).

[Peng, Xu 2005] K. Peng, Y. Xu, Y. Wu, Y. Yan, S.-T. Lee, J. Zhu. Aligned single-crystalline Si nanowire arrays for photovoltaic applications. *Small* 1, 1062 (2005).

[Peng, 2006] K.Q. Peng, J.J. Hu, Y.J. Yan, H. Fang, Y. Xu, S.T. Lee, J. Zhu. Fabrication of single crystalline silicon nanowires by scratching a silicon surface with catalytic metal particles. *Adv. Funct. Mater*. 16, 387 – 94 (2006).

[Peng, 2007] K. Peng, M. Zhang, A. Lu, N.B. Wong, R. Zhang, S.T. Lee. Ordered silicon nanowire arrays via nanosphere lithography and metal-induced etching. *Appl. Phys. Lett.* 90, 163123 (2007).

[Presti, 2006] C.D. Presti, A. Irrera, G. Franzò, I. Crupi, F. Priolo, F. Iacona, G. Di Stefano, A. Piana, D. Sanfilippo, P. G. Fallica. Photonic-crystal silicon-nanocluster light-emitting device. *Appl. Phys. Lett*. 88, 033501 (2006).

[Prokes, 1995] S.M. Prokes, W.E. Carlos. Oxygen defect center red room temperature photoluminescence from freshly etched and oxidized porous silicon. J. Appl. Phys. 78, 2671 (1995).

[Prokes, 1996] S.M. Prokes. Surface and optical properties of porous silicon. *J. Mater. Res*. 11, 305 – 20 (1996).

[Qin, 1993] G.G. Qin, Y.Q. Jia. Mechanism of the visible luminescence in porous silicon. *Solid State Comm*. 86, 559 – 63, (1993).

[Qiu, 2005] T. Qiu, X.L. Wu, X. Yang, G.S. Huang, Z.Y. Zhang. Self-assembled growth and optical emission of silver-capped silicon nanowires. *Appl. Phys. Lett*. 84, 3867 (2005).

[Qu, 2009] Y. Qu, L. Liao, Y. Li, H. Zhang, Y. Huang, X. Duan. Electrically conductive and optically active porous silicon nanowires. *Nano Lett*. 9, 4539 – 43 (2009).

[Robinson, 1993] M. B. Robinson, A. C. Dillon, and S. M. George. Porous silicon photoluminescence versus HF etching: No correlation with surface hydrogen species. *Appl. Phys. Lett*. 62, 1493 – 95 (1993).

[Ross, 2005] F. M. Ross, J. Tersoff, M. C. Reuter. Sawtooth faceting in silicon nanowires. *Phys. Rev. Lett*. 95, 146104 (2005).

[Sacilotti, 1993] M. Sacilotti, P. Abraham, B. Champagnon, Y. Monteil, J. Bouix. Porous silicon photoluminescence: type II-like recombination mechanism. *Electr. Lett*. 29, 790 – 91 (1993).

[Schmidt, 2005] V. Schmidt, S. Senz, U. Gösele. Diameter-dependent growth direction of epitaxial silicon nanowires. *Nano Letters* 5, 931 - 35 (2005).

[Sivakov, 2006] V. Sivakov, G. Andrä, C. Himcinschi, U. Gösele, D.R.T. Zahn, S.H. Christiansen. Growth peculiarities during vapor–liquid–solid growth of silicon nanowhiskers by electron-beam evaporation. *Appl. Phys. A* 85, 311 - 15 (2006).

[Sivakov, 2007] V. Sivakov, F. Heyroth, F. Falk, G. Andrä, S.H. Christiansen. Silicon nanowire growth by electron beam evaporation: Kinetic and energetic contributions to the growth morphology. *J. Cryst. Growth* 300, 288 – 93 (2007).

[Sivakov, 2009] V. Sivakov, G. Andrä, A. Gawlik, A.Berger, J. Plentz, F. Falk, S.H. Christiansen. Silicon nanowire based solar cells on glass: synthesis, optical properties, and cell parameters. *Nano Letters* 9, 1549 – 54 (2009).

[Sivakov, 2010] V.A. Sivakov, G. Brönstrup, B. Pecz, A. Berger, G.Z. Radnoczi, M. Krause, S.H. Christiansen. Realization of vertical and zigzag single crystalline silicon nanowire architectures. *J. Phys. Chem. C* 114, 3798 – 3803 (2010).

[Sivakov, Voigt, 2010] V.A. Sivakov, F. Voigt, A. Berger, G. Bauer, S.H. Christiansen. Roughness of silicon nanowire sidewalls and room temperature photoluminescence. *Phys. Rev. B* 82, 125446 (2010).

[Skuja, 1979] L.N. Skuja, A.R. Silin. Optical properties and energetic structure of non-bridging oxygen centers in vitreous SiO_2. *Physica Status Solidi A* 56, K11–K13 (1979).

[Stelzner, 2008] Th. Stelzner, M. Pietsch, G. Andrä, F. Falk, E. Ose, S.H. Christiansen. Silicon nanowire-based solar cells. *Nanotechnology* 19, 295203 (2008).

[Stesmans, 1994] A. Stesmans, F. Scheerlinck. Natural intrinsic EX center in thermal SiO_2 on Si: ^{17}O hyperfine interaction. *Physical Review B* 50, 5204-5212 (1994).

[Street, 1991] R.A. Street. Hydrogenated amorphous silicon. Cambridge: Cambridge University Press (1991).

[Sunkara, 2001] M.K. Sunkara, S. Sharma, and R. Miranda. Bulk synthesis of silicon nanowires using a low temperature vapor–liquid–solid method. *Appl. Phys. Lett*. 79, 1546 (2001).

[Tsai, 1991] C. Tsai, K.-H. Li, J. Sarathy, S. Shih, and J. C. Campbell, B. K. Hance, J.M. White. Thermal treatment studies of the photoluminescence intensity of porous silicon. *Appl. Phys. Lett*. 59, 2814 – 16 (1991).

[Tsakalakos, 2007] L. Tsakalakos, J. Balch, J. Fronheiser, M. Shih, S. LeBoeuf, M. Pietrzykowski, P. Codella, B. Korevaar, O. Sulima, J. Rand & others. Strong broadband optical absorption in silicon nanowire films. *J. Nanophotonic* 1, 013552 (2007).

[Tsakalakos, Balch, 2007] L. Tsakalakos, J. Balch, J. Fronheiser, A. Korevaar, O. Sulima, J. Rand. Silicon nanowire solar cells. *Appl. Phys. Lett.* 91, 233117 (2007).

[Uhlir, 1956] A. Uhlir. Electrolytic shaping of germanium and silicon. *Bell. Syst. Tech. J.* 35, 333 (1956).

[Vetterl, 2000] O. Vetterl, F. Finger, R. Carius, P. Hapke, L. Houben, O. Kluth, A. Lambertz, A. Mück, B. Rech, H. Wagner. Intrinsic microcrystalline silicon: A new material for photovoltaics. *Solar Energy Materials and Solar Cells* 62, 97-108 (2000).

[Voigt, 2011] F. Voigt, V. Sivakov, V. Gerliz, G. H. Bauer, B. Hoffmann, G. Z. Radnoczi, B. Pecz, S. Christiansen. Photoluminescence of samples produced by electroless wet chemical etching: Between silicon nanowires and porous structures. Physica Status Solidi A 208, 893 (2011).

[Wagner, 1961] C. Wagner. Theorie der Alterung von Niederschlägen durch Umlösen (Ostwald-Reifung). *Z. Elektrochem*. 65, 581 - 91 (1961).

[Wagner@Ellis, 1964] R. S. Wagner, W. C. Ellis. Vapor-solid-liquid mechanism of single crystal growth. *Appl.Phys. Lett*. 4, 89 (1964).

[Wagner@Ellis, 1965] R. S. Wagner, W. C. Ellis. The vapor-liquid-solid mechanism of crystal growth and its application to silicon. *Trans. Metall. Soc. AIME* 233, 1053 - 64 (1965).

[Walavalkar, 2010] S. S. Walavalkar, C. E. Hofmann, A. P. Homyk, M. D. Henry, H. A. Atwater, A. Scherer. Tunable visible and near-IR emission from sub-10 nm etched single-crystal Si nanopillars. *Nano Lett.* 10, 442328 (2010).

[Wang, 2006] Y. Wang, V. Schmidt, S. Senz , U. Gösele. Epitaxial growth of silicon nanowires using an aluminium catalyst. *Nature Nanotechnology* 1, 186 - 189 (2006).

[Weiss, 1935] J. Weiss. The catalytic decomposition of hydrogen peroxide on different metals. *Trans. Faraday Soc.* 31, 1547- 57 (1935).

[Wiegel, 1930] E. Wiegel. Über Farbe und Teilchengröße von kolloidem Silber, insbesondere der neuen Wasserstoffperoxydsilbersole Colloid & Polymer Science 53, 96-101 (1930).

[Wilson@Hutley, 1982] S. Wilson, M. Hutley. The optical properties of 'Moth Eye' antireflection surfaces. *J. Modern Opt*. 29, 993 – 1009 (1982).

[Wolford, 1983] D. J. Wolford, B. A. Scott, J. A. Reimer, J. A. Bradley. Efficient visible luminescence from hydrogenated amorphous silicon. *Physica B+C* 117-118, 920-22 (1983).

[Wu, 2000] Y. Wu, P. Yang. Germanium nanowire growth via simple vapor transport. *Chem. Mater*. 12, 605 – 07 (2000).

[Xia, 2003] Y. Xia, P. Yang, Y. Sun, Y. Wu, B. Mayers, B. Gates, Y. Yin, F. Kim, H. Yan. One-dimensional nanostructures: Synthesis, characterization, and applications. *Adv. Mater.* 15, 353 - 89 (2003).

[Zhang, 2000] Y. F. Zhang, Y. H. Tang, N. Wang, C. S. Lee, I. Bello, S. T. Lee. Germanium nanowires sheathed with an oxide layer. *Phys. Rev. B* 61, 4518 - 21 (2000).

[Zhang, 2008] M.-L. Zhang, K.-Q. Peng, X. Fan, J.-S. Jie,R.-Q. Zhang, S.-T. Lee, N.-B. Wong. Preparation of large area uniform silicon nanowires arrays through metal-assisted chemical etching. *J. Phys. Chem. C* 112, 4444 - 50 (2008).

Nanowires - Fundamental Research

Edited by Dr. Abbass Hashim

ISBN 978-953-307-327-9
Hard cover, 552 pages
Publisher InTech
Published online 19, July, 2011
Published in print edition July, 2011

Understanding and building up the foundation of nanowire concept is a high requirement and a bridge to new technologies. Any attempt in such direction is considered as one step forward in the challenge of advanced nanotechnology. In the last few years, InTech scientific publisher has been taking the initiative of helping worldwide scientists to share and improve the methods and the nanowire technology. This book is one of InTechâ€™s attempts to contribute to the promotion of this technology.

How to reference

In order to correctly reference this scholarly work, feel free to copy and paste the following:

Vladimir Sivakov, Felix Voigt, Björn Hoffmann, Viktor Gerliz and Silke Christiansen (2011). Wet - Chemically Etched Silicon Nanowire Architectures: Formation and Properties, Nanowires - Fundamental Research, Dr. Abbass Hashim (Ed.), ISBN: 978-953-307-327-9, InTech, Available from: http://www.intechopen.com/books/nanowires-fundamental-research/wet-chemically-etched-silicon-nanowire-architectures-formation-and-properties

INTECH
open science | open minds

InTech Europe
University Campus STeP Ri
Slavka Krautzeka 83/A
51000 Rijeka, Croatia
Phone: +385 (51) 770 447
Fax: +385 (51) 686 166
www.intechopen.com

InTech China
Unit 405, Office Block, Hotel Equatorial Shanghai
No.65, Yan An Road (West), Shanghai, 200040, China
中国上海市延安西路65号上海国际贵都大饭店办公楼405单元
Phone: +86-21-62489820
Fax: +86-21-62489821

IntechOpen